

DIPLOMARBEIT

Performance enhancement in CWDM systems

ausgeführt am Institut für
Nachrichtentechnik und Hochfrequenztechnik der
Technischen Universität Wien
von

Perica Jurčević

Rotenturmstrasse 25/9
1010 Wien

Matrikelnummer 9826825

Wien, im Mai 2008

Betreuer:

Dr. Franz Fidler
Prof. Dr. Walter R. Leeb

Danksagung

Ich möchte mich bei allen bedanken, die durch ihre fachliche und persönliche Unterstützung zum Gelingen dieser Diplomarbeit beigetragen haben.

Ich danke meinen Eltern, Mira und Ivan Jurčević, die mir das Studium der Elektrotechnik ermöglicht haben.

Herzlichen Dank an Prof. Dr. Walter Leeb, Vorstand des Instituts für Nachrichten- und Hochfrequenztechnik, für die zahlreichen Anregungen im Bezug auf diese Diplomarbeit.

Ganz besonders möchte ich mich bei Herrn Dr. Franz Fidler bedanken, für die ausgezeichnete Betreuung, die vielen aufschlussreichen Diskussionen und Ratschläge sowie seine kollegiale Unterstützung während der Durchführung dieser Diplomarbeit.

Ich danke meiner Freundin Ranka Čelić, meinem Bruder Goran Jurčević sowie allen lieben Freunden und Studienkollegen die mich während meines Studiums immer unterstützt haben.

Perica Jurčević

Kurzfassung

Die Forderung nach immer höheren Bitraten im Netzzugangsbereich des Internet führt zum vermehrten Einsatz von optischen Verteilsystemen. Damit diese auch vom ökonomischen Standpunkt aus gesehen rentabel sind ist es notwendig kostengünstige Komponenten zu verwenden und deren Verhalten im System zu untersuchen. Die Einführung von vertikal emittierenden Lasern (VCSELs) bei Wellenlängen um 1550 nm und deren Potenzial zur kostengünstigen Massenproduktion begünstigen deren Einsatz gegenüber z.B. DFB Lasern. Empfindliche optische Empfänger mit Lawinenphotodioden und optischen Halbleiterverstärkern (SOAs) können zur Steigerung der Übertragungsdistanz verwendet werden. Um eine bessere Ausnutzung der Faser zu erreichen werden heute mehrere Wellenlängen gleichzeitig zur Informationsübertragung in sogenannten Wellenlängenmultiplex System (WDM) verwendet. In CWDM Systemen wird dabei mit einem relativ breiten Kanalabstand von 20 nm gearbeitet, der es ermöglicht die temperaturabhängige Emissionswellenlängenverschiebung der VCSELs zu tolerieren.

Das Ziel meiner Arbeit war die Charakterisierung der Laserquellen und deren Modifikation damit diese bei einer Bitrate von 10.7 Gb/s statt bei den von den Herstellern spezifizierten 2.5 Gb/s betrieben werden können. Weiters wurde ein Vergleich von PIN und APD Diode durchgeführt und deren Empfindlichkeiten messtechnisch erfasst. Der Einsatz eines SOAs, sollte eine weitere Erhöhung der maximalen Übertragungsdistanz ermöglichen. Die erreichbaren Übertragungsdistanzen über single modige Glasfasern bei Bitraten von 1, 2.5 und 10.7 Gb/s wurden ermittelt und festgestellt ob die Dämpfung oder die Dispersion die Reichweiten limitieren. Zuletzt wurde die Übertragung eines HD-SDI Videosignals mit einer Datenrate von 1.485 Gb/s durchgeführt und die dabei maximal erreichbare Übertragungsdistanz ermittelt.

Beim Vergleich der Empfindlichkeit der Empfänger mit APD oder PIN Diode bei 10.7 Gb/s wurde ein Gewinn von 10 dB mit der APD im Vergleich zur PIN Diode festgestellt. Bei 2.5 Gb/s und 1 Gb/s wurden jeweils 13 und 13.5 dB erreicht. Am Ausgang des SOA wurde eine relativ hohe Rauschleistung von 3.8 mW gemessen, verursacht durch die verstärkte spontane Emission (ASE) in der aktiven Zone des Verstärkers. Diese hohe Rauschleistung führte dazu, dass die erreichten Reichweiten unter Verwendung des SOA um bis zu 10 km geringer waren als ohne. Die Messergebnisse im Einkanalssystem zeigten eine starke Abhängigkeit von der Länge der verwendeten Pseudo-Zufallsfolge (PRBS) auf. Diese Pattern-Abhängigkeit lässt den Schluss zu, Codes zu verwenden welche lange Serien von Einsen und Nullen vermeiden, um damit die Übertragungsdistanz zu maximieren. So wurde bei 10.7 Gb/s eine Übertragungsdistanz von 88 km mit einer PRBS der Länge $2^7 - 1$ erreicht, während mit einer $2^{31} - 1$ PRBS nur 66 km möglich waren. Bei 2.5 Gb/s und 1 Gb/s wurden jeweils Übertragungsdistanzen von 130 km und 150 km erzielt. Im Gesamtsystem mit einer Datenrate von 10.7 Gb/s und einer Bitfehlerwahrscheinlichkeit von 10^{-3} konnte bei Verwendung der APD eine Steigerung um 13 km gegenüber dem System mit PIN Diode verzeichnet und somit die Dispersionsbegrenzung des Systems erreicht werden. Das hochauflösende HD-SDI Videosignal konnte über eine Distanz von 107 km im Einkanalfall und über 102 km im Mehrkanalfall fehlerfrei übertragen werden.

Abstract

The increasing demand for higher bit rates in the network access area of the Internet leads to an increase of optical distribution systems. From an economical point of view it is necessary to use low cost components and investigate their behaviour in the system. The introduction of vertical cavity surface emitting lasers (VCSELs) at wavelengths around 1550 nm and their potential for cost effective mass production favours their use when compared to e.g. DFB lasers. Sensitive optical receivers with avalanche photo diodes and semiconductor optical amplifiers (SOAs) can be used to increase the transmission distance. Nowadays, often a simultaneous transmission of information over several different wavelengths in a so called wavelength division multiplexing system is used. CWDM systems use a relatively wide channel spacing of 20 nm, which allows to tolerate the temperature dependent emission wavelength shift of the VCSELs.

The goal of my work was the characterization of the laser sources and their modification to enable their operation at a bit rate of 10.7 Gb/s instead of the 2.5 Gb/s which was specified by the vendor. Furthermore, a comparison of the PIN and APD diode was performed and their sensitivities were measured. The implementation of an SOA in the system should allow a further increase of the maximum transmission distance. The achievable transmission distance over single mode fiber at bit rates of 1, 2.5, and 10.7 Gb/s were measured and it was determined whether the attenuation or the dispersion limit the maximum reach. Finally, the transmission of an HD-SDI video signal at a data rate of 1.485 Gb/s was performed and the maximum achievable transmission distance was measured.

A comparison of the sensitivities of the receivers with APD and with PIN diode at 10.7 Gb/s showed a gain of 10 dB with an APD compared to the case when a PIN diode was used. At 2.5 Gb/s and 1 Gb/s a gain of 13 and 13.5 dB was achieved respectively. At the output of the SOA a relatively high noise power of 3.8 mW was measured, which is caused through amplified spontaneous emission (ASE) in the active zone of the amplifier. This high noise power led to an up to 10 km shorter transmission distance in comparison to the case without the SOA. Measurements in the single channel system revealed a strong bit pattern dependence of the maximum reach. This pattern dependence led to the conclusion that a coding scheme which prevents long runs of ones or zeros helps to increase the achievable transmission distance. For example at 10.7 Gb/s a transmission distance of 88 km was achieved with a pseudo random bit sequence (PRBS) length of $2^7 - 1$, while with a PRBS length of $2^{31} - 1$ only a distance of 66 km was achieved. At 2.5 Gb/s and 1 Gb/s transmission distances of 130 km and 150 km were measured. In the 4 channel CWDM system at a data rate of 10.7 Gb/s and a bit error ratio of 10^{-3} an increase of 13 km in transmission distance was possible when using an APD instead of a PIN diode, thereby reaching the dispersion limit of the system. The HD-SDI video signal could be transmitted without error over a distance of 107 km in the single channel case and over 102 km in the 4 channel CWDM system.

Contents

1	Introduction to CWDM	1
2	Characterization of the components of the CWDM system	4
2.1	Vertical-cavity surface-emitting lasers (VCSELs)	5
2.1.1	Static properties of the VCSELs	5
2.1.2	Dynamic properties of the VCSELs	13
2.2	Receivers	15
2.2.1	APD Diode	15
2.2.2	PIN Diode	23
2.2.3	Comparison of the performance of the PIN- and APD- Diode	24
2.3	Semiconductor optical amplifier (SOA)	26
2.3.1	Static properties of the SOA	26
2.3.2	Dynamic properties of the SOA	29
2.4	Multiplexer and demultiplexer	31
2.5	Optical 3 dB splitter	33
2.6	Standard single mode fiber	33
3	CWDM system performance	35
3.1	Single channel performance	35
3.1.1	System setup for the single channel measurements	35
3.1.2	Measurement results at 10.7 Gb/s	36
3.1.3	Measurement results at 2.5 Gb/s	38
3.1.4	Measurement results at 1 Gb/s	41
3.2	4-channel CWDM system performance	44
3.2.1	Measurement results at 10.7 Gb/s	44
3.2.2	Measurement results at 2.5 Gb/s	46
3.2.3	Measurement results at 1 Gb/s	48
3.3	HD-video transmission via CWDM system	50
3.4	Conclusion	53
	Appendices	54
	Appendix A	55
	Datasheets	55
A1.	APD diode (AT10XGC)	55
A2.	PIN diode (R2860C)	56
A3.	SOA (BOA1004)	56

Abbreviations	58
Bibliography	60

Chapter 1

Introduction to CWDM

Data traffic over the Internet increases very fast and doubles approximately every 6 to 12 months [1]. This is due to the fast spreading of commercial applications like video streaming, Internet radio, MP3, file sharing, and IP-telephony to name just a few and of course to the ever increasing amount of users in the Internet. For long haul transmission fiber optic cables are already used for quite a long time. Whereas the connection to the end user is usually done via electrical wire. The limited bandwidth of electrical lines led to the development of technologies like integrated services digital network (ISDN) and asynchronous digital subscriber line (ADSL) for the better utilization of this restricted resource. Today it is getting harder and harder to keep up with the growing bandwidth demand while having a bottleneck which is the connection to the end user. To keep up with this fast growing demand for data bandwidth new strategies have to be developed. One is to use a fiber optic cable that offers a great amount of bandwidth when compared with electrical cables. Additionally, wavelength division multiplexing (WDM) can be used to increase the data traffic through an optical fiber by transmitting data with several lasers at different wavelengths. In Figure 1.1 you can see the basic setup of an WDM system, where the signals of several laser sources at different wavelengths are coupled through a multiplexer onto one standard single mode fiber. At the receiving end the signal is demultiplexed via a demultiplexer and then transformed into an electrical signal by the photodiodes. The data rate

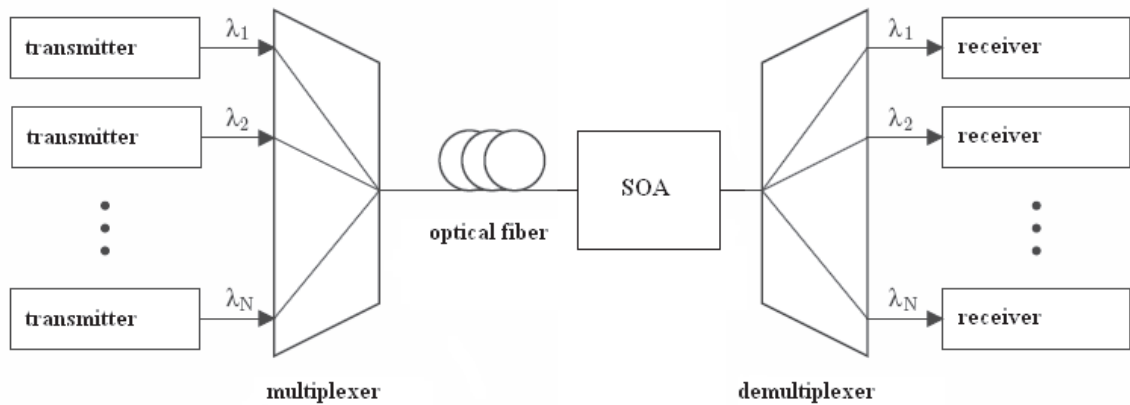


Figure 1.1: Basic CWDM system setup (SOA...semiconductor optical amplifier)

transmitted over the fiber is the sum of the data rates in each channel. The achieved accumulated data rate equals to:

$$R_{acc} = R_1 + R_2 + + R_N. \quad (1.1)$$

Concerning the overall system one can distinguish between dense wavelength division multiplexing (DWDM) and coarse wavelength division multiplexing (CWDM). The three possible channel spacing in DWDM systems is defined in the ITU-T G.694.1 [2] frequency grid. The three channel spacings defined in this standard are 100 GHz, 50 GHz, and 25 GHz. A frequency of 193.10 THz (1552.52 nm) is chosen as the reference frequency. Because of the definition of the channel spacing in the frequency domain it follows that the spacing in terms of wavelength is different for each channel. The channel spacing in the wavelength domain can be calculated to:

$$\Delta\lambda = \Delta f \frac{\lambda}{f} \quad (1.2)$$

where λ and f are the center wavelength and frequency of the calculated channel. CWDM defines its channel spacing in the wavelength domain, one channel has a width of 20 nm [2]. The center wavelengths of the CWDM system start at 1271 nm and stop at 1610 nm which is shown in Figure 1.2. An illustration of the channel packaging of DWDM compared with CWDM can be seen in Figure 1.3 for a DWDM channel spacing of 100 GHz. In this case 25 DWDM channels fit into 1 CWDM channel. DWDM systems have to maintain more stable wavelength or frequency than those needed for CWDM because of the closer spacing of the channels. Precision temperature control of the lasers is required in DWDM systems to prevent a drifting out of the very narrow frequency window. Since DWDM provides greater maximum capacity it tends to be used at a higher level in the communications hierarchy than CWDM, for example on the Internet backbone and is therefore associated with higher modulation rates. CWDM is meant for last mile applications like fiber to the home (FTTH), fiber to the curb (FTTC), or fiber to the building (FTTB) i.e. high data rate access over optical fiber for private homes.

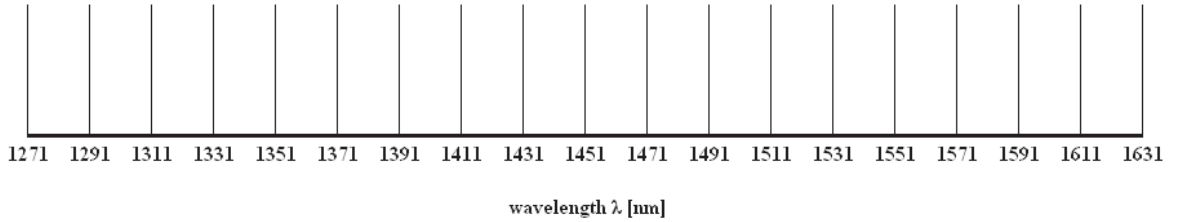


Figure 1.2: CWDM wavelength channels according to [2] (CWDM...coarse wavelength division)

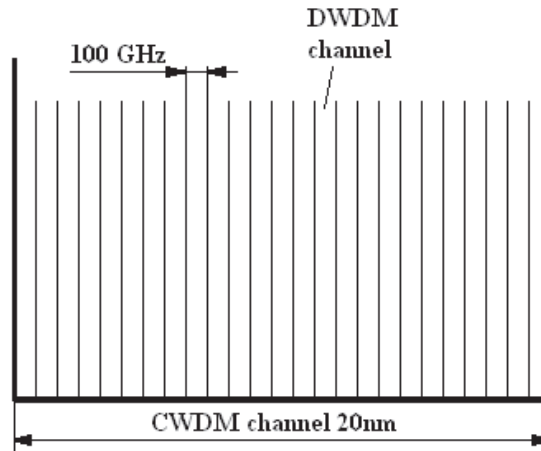


Figure 1.3: Comparison of CWDM [2] with DWDM [3] wavelength channels (CWDM...coarse wavelength division multiplexing, DWDM...dense wavelength division multiplexing).

This work is a successor of the diploma theses [4] [5] [6] where a CWDM system was built using DFB lasers [5], a new and cheap laser source - namely a vertical-cavity surface emitting laser (VCSEL) was characterized in detail in [6], and a CWDM system was built and tested using such VCSELs [4]. The main goal of my work is to increase the transmission distance by using additional components such as avalanche photo diodes (APDs) instead of positive intrinsic negative (PIN) diodes and semiconductor optical amplifiers (SOAs). Using this measures I want to overcome the attenuation limit and reach the dispersion limited distance of the system.

Chapter 2

Characterization of the components of the CWDM system

The following chapter describes the characteristics of the components of the CWDM system. Figure 2.1 shows the setup of the CWDM system consisting of uncooled directly modulated lasers as light sources which are modulated with a data rate of up to 10.7 Gb/s depending on the laser used. The optical data streams of the lasers are then multiplexed via a thin-film multiplexer into a standard single mode fiber (SSMF) and transmitted over a certain distance. The optical fiber attenuates the signal with increasing fiber length. To achieve a higher transmission distance I investigated the use of a semiconductor optical amplifier within the system. At the receiving end of the transmission link I use a thin-film demultiplexer to separate the different wavelengths and guide them to the corresponding receiver. For the detection and conversion of the optical signal into an electrical signal I use PIN or APD diodes. Where the latter offer a greater sensitivity and therefore the potential to achieve a larger transmission distance.

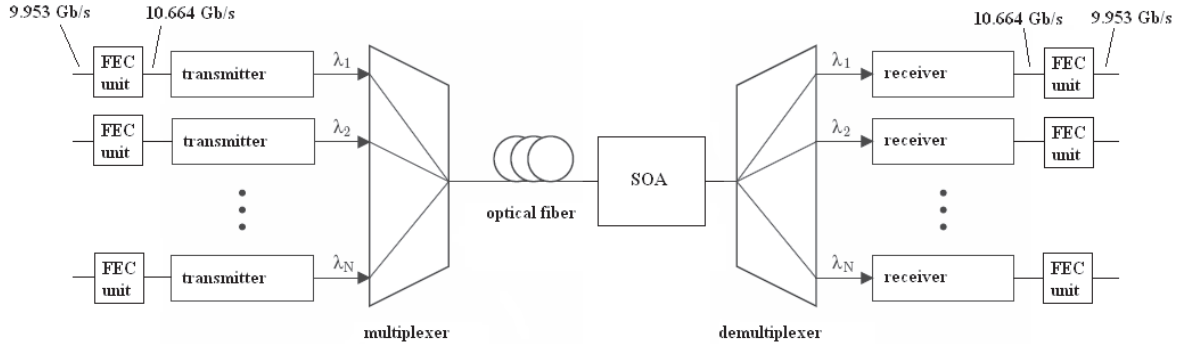


Figure 2.1: CWDM system with forward error correction (SOA...semiconductor optical amplifier).

Figure 2.1 also shows a forward error correction (FEC) used to correct bit errors which can occur during transmission. By adding overhead information to the payload data stream these errors can be detected and corrected by the FEC. The overhead of the FEC in the case of the synchronous optical network (SONET) standard is 7% which makes it necessary to transmit at a data rate of 10.664 Gb/s instead of 9.953 Gb/s. The use of an FEC enables the recovery of a received datastream with a BER of 10^{-3} to a BER of 10^{-15} [7] [8] [9] and thereby increasing the maximum transmission distance. These FEC units were not implemented in the measurements performed in this work. However, the measurements were performed at a bitrate of 10.7 Gb/s and aimed to achieve a bit error rate (BER) of 10^{-3} having in mind that when using FEC the BER can be recovered to 10^{-15} as long as no burst errors occur.

2.1 Vertical-cavity surface-emitting lasers (VCSELs)

Distributed feedback (DFB) lasers are commonly used in the long wavelength range around 1550 nm. Another possible laser source, namely vertical surface emitting lasers (VCSELs), have the potential of low cost mass production but became available just recently in the long wavelength area. That VCSELs at this wavelength are very new to the market is also shown by the circumstance that there are only two different vendors worldwide, namely RayCan [10] and Vertilas [11], who produce them. As transmitters for the CWDM system I use VCSELs in the 1550 nm wavelength area, because the SSMF has its lowest attenuation there. These lasers are initially specified by the vendors up to a data rate of 2.5 Gb/s and eye diagrams with clear eye opening up to 5 Gb/s. The Vertilas VCSELs were already used in previous diploma theses at higher data rates [4] [6] where they were modified to work at a bit rate of up to 10.7 Gb/s. The purchased lasers were not preselected and the measured center wavelengths of the lasers are displayed in Table 2.1 showing that three of the RayCan lasers were within the 1531 nm CWDM band while one was situated in the 1511 nm CWDM band.

Vertilas	RayCan
1531 nm	1515 nm
1551 nm	1524 nm
1571 nm	1531 nm
1591 nm	1538 nm

Table 2.1: Emission wavelengths of the lasers used in the system.

The Vertilas VCSELs all occupied different adjacent CWDM bands. An image of the RayCan VCSEL mounted onto a 50 Ω microstrip line can be seen in Figure 2.2(a) while one of the Vertilas VCSELs is shown in Figure 2.2(b). An SMA connector is used for easy connection of the lasers. Since the properties of the Vertilas lasers have already been measured in a previous work [4] I will concentrate here on the RayCan lasers and present only a few results from [4] for comparison.

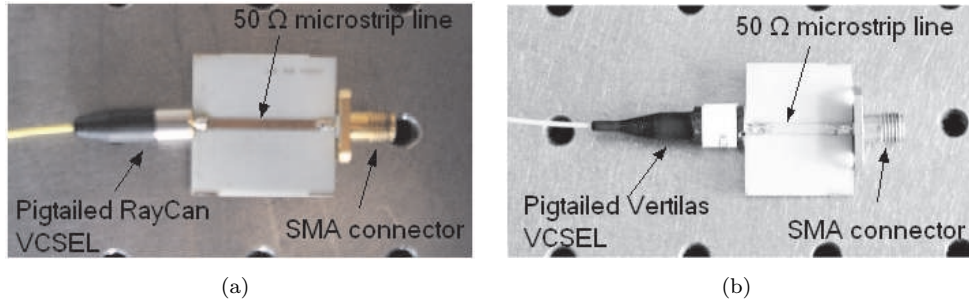


Figure 2.2: Pigtailed VCSEL mounted on 50 Ω microstrip line a) RayCan and b) Vertilas.

2.1.1 Static properties of the VCSELs

The measurement setup for the static properties of the VCSELs can be seen in Figure 2.3. The current source PRO800 is used to bias the VCSEL as well as to measure the voltage with a built in voltmeter. The VCSEL's optical output power is measured with the optical power meter ML9108 with sensor MA9302A which is sensitive in the range of 750 to 1800 nm. The spectrum is taken with the optical spectrum analyzer AQ6319. I did not use a power splitter to assure more accurate measurements. To regulate the VCSEL's ambient temperature it is put in a climatic chamber.

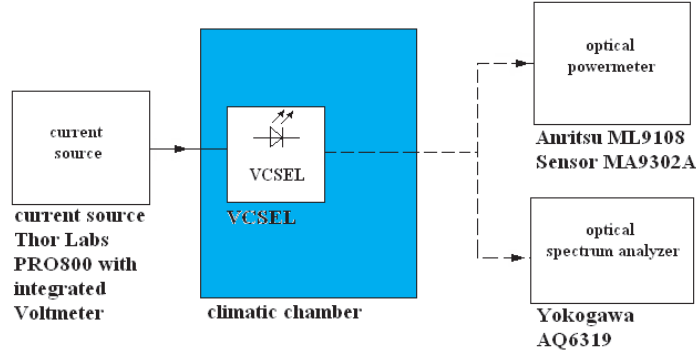


Figure 2.3: Setup for the measurement of the static properties of the VCSELs.

Static characteristics of the 1515 nm RayCan VCSEL

Figure 2.5(a) depicts the optical output power versus the laser current of an 1515 nm RayCan VCSEL as a function of the ambient temperature. The optical output power of the laser decreased rapidly with increasing temperature, which is mainly caused by an additional coupling loss into the fiber [4]. The electrical characteristics depicted in Figure 2.5(b) remain relatively independent from the ambient temperature. The variation of the output power with temperature is $7.5 \mu\text{W/K}$ at a bias current of 6 mA. The dependence of the emitted laser wavelength from the laser current is depicted in Figure 2.5(c). The curves were measured at various temperatures. The covered wavelength range is between 1513.5 nm and 1522.1 nm corresponding to 0.133 nm/K , which is not always within the 1511 nm band (which is from 1501 nm to 1521 nm). Since the optimum bias current is found at 6 mA, the covered wavelength at this bias current is 1515.5 to 1519.5 nm which again is within the specified 1511 nm band. The threshold current versus ambient temperature can be seen in Figure 2.5(d) corresponding to a shift of 1 mA when changing the temperature from 20°C to 50°C (which can also be observed in Figure 2.5(a)). A list of slope efficiencies $E_s = \frac{\Delta P}{\Delta I}$ and differential resistances $R_d = \frac{\Delta U}{\Delta I}$ at 6 mA bias current for different temperatures can be seen in Table 2.2. The slope efficiency is defined as the slope of the optical power versus laser current curve, and it shows the sensitivity of the optical laser output to a modulation by the laser current. Figure 2.4 displays the plot of the optical power versus current and voltage versus current of the 1511 nm Vertilas VCSEL. The main difference to the RayCan VCSELs is a higher output power and a larger slope efficiency of 0.18 W/A . From the U-I-curve it is seen that the power consumption of the Vertilas VCSEL is lower then for the RayCan device.

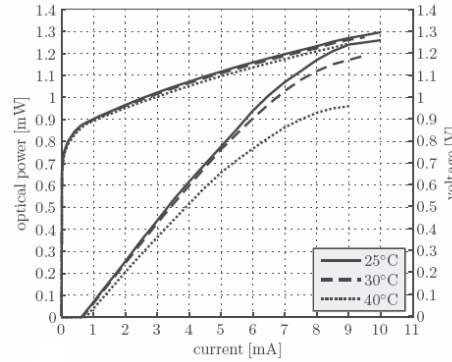


Figure 2.4: U-I and P-I characteristics of the Vertilas 1511 nm VCSEL.

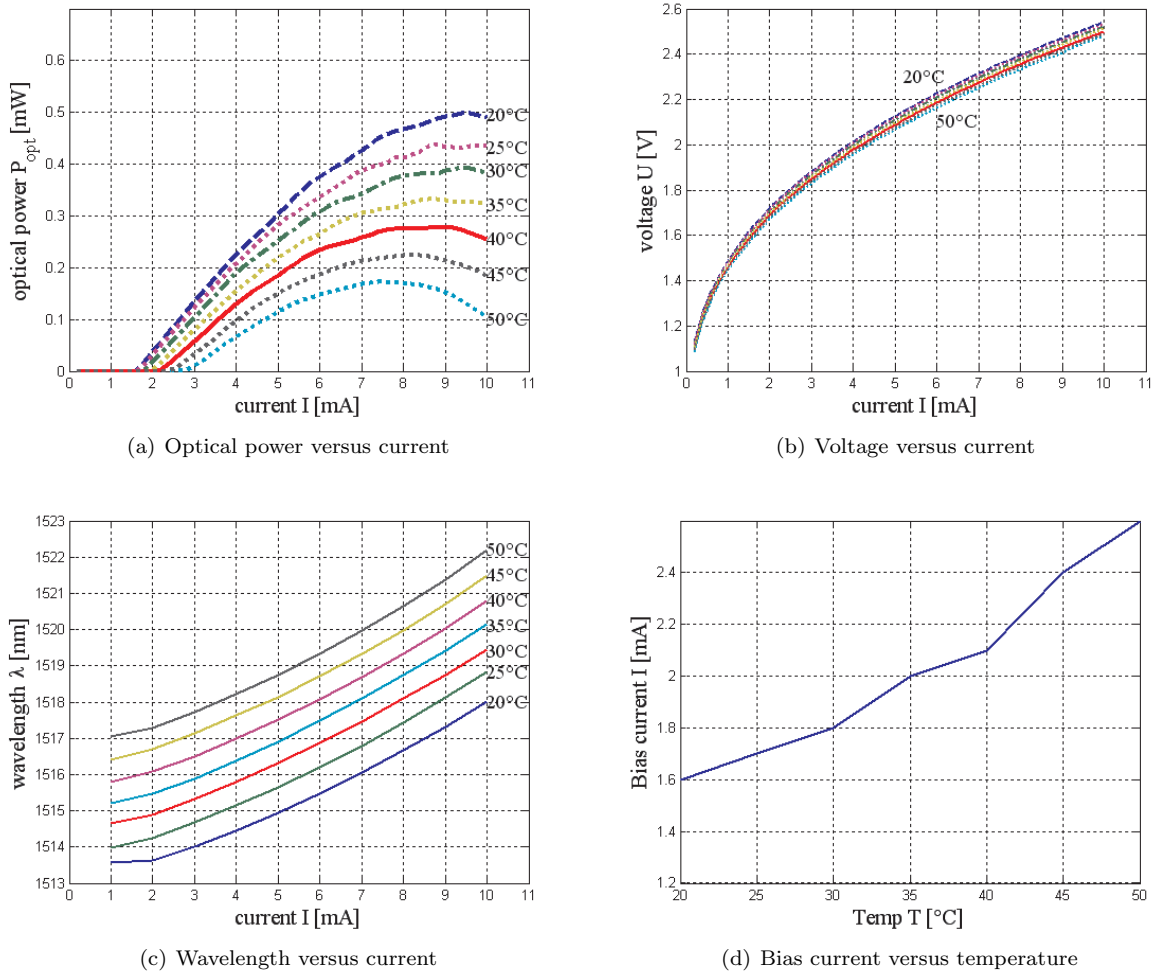


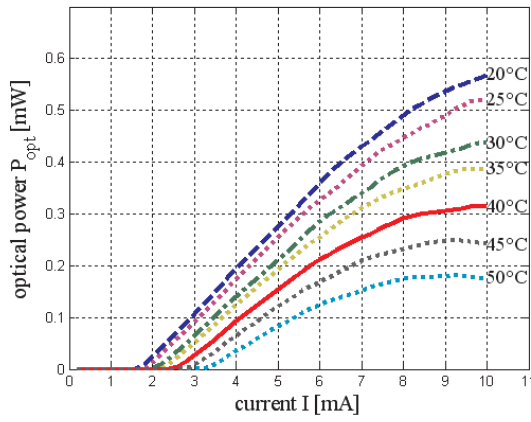
Figure 2.5: Static characteristics at various temperatures of the 1515 nm RayCan VCSEL: a) P-I characteristics, b) U-I characteristics, c) wavelength versus laser current d) threshold current versus temperature.

Temp[°C]	E_s [W/A]	R_d [Ω]
20	0.05804	91.6
25	0.05049	91.5
30	0.04098	91.3
35	0.04273	91.1
40	0.03294	90.9
45	0.02937	90.7
50	0.02168	90.5

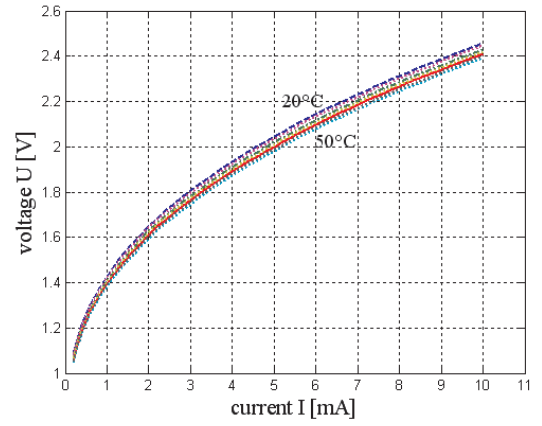
Table 2.2: Slope efficiency E_s and differential resistance R_d of the 1515 nm RayCan VCSEL as a function of the ambient temperature.

Static characteristics of the 1524 nm RayCan VCSEL

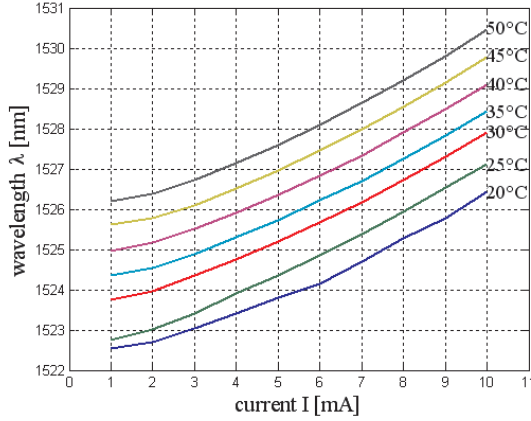
Figure 2.6(a) depicts the optical output power versus the laser current of an 1524nm RayCan VCSEL as a function of the ambient temperature. The 1524nm center wavelength of the laser is very close to the lower edge of the 1531 nm wavelength band, which is at 1521 nm. The covered wavelength range can be seen from Figure 2.6(c) to range from 1522.5 to 1530.5 nm which is entirely within the 1531 nm band. The variation of the output power with temperature is $8 \mu\text{W/K}$ at a bias current of 6 mA. Figure 2.5(d) shows the threshold current versus ambient temperature with a shift of 1 mA when changing the temperature from 20°C to 50°C (which can also be observed in Figure 2.6(a)). Table 2.3 shows a list of slope efficiencies $E_s = \frac{\Delta P}{\Delta I}$ and differential resistances $R_d = \frac{\Delta U}{\Delta I}$ at 6 mA bias current for different temperatures.



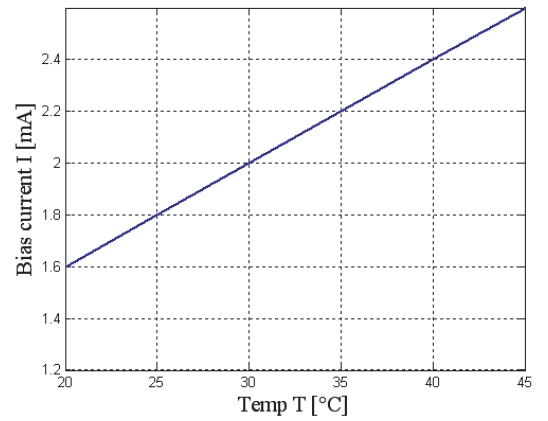
(a) Optical power versus current



(b) Voltage versus current



(c) Wavelength versus current



(d) Bias current versus temperature

Figure 2.6: Static characteristics at various temperatures of the 1524nm RayCan VCSEL: a) P-I characteristics, b) U-I characteristics, c) wavelength versus laser current d) threshold current versus temperature.

Temp[°C]	E_s [W/A]	R_d [Ω]
20	0.06713	92.1
25	0.06503	91.3
30	0.05734	90.7
35	0.05244	90.0
40	0.04406	89.3
45	0.03636	88.3
50	0.03147	87.2

Table 2.3: Slope efficiency E_s and differential resistance R_d of the 1524 nm RayCan VCSEL as a function of the ambient temperature.

Static characteristics of the 1531 nm RayCan VCSEL

Figure 2.7(a) depicts the optical output power versus the laser current of an 1531 nm RayCan VCSEL as a function of the ambient temperature. The covered wavelength range can be seen from Figure 2.7(c) to be from 1529.6 to 1537.9 nm which is entirely within the 1531 nm band. The variation of the output power with temperature is $6.3 \mu\text{W/K}$ at a bias current of 6 mA. Figure 2.5(d) shows the threshold current versus ambient temperature with a shift of 1 mA when changing the temperature from 20 °C to 50 °C (which can also be observed in Figure 2.6(a)). Table 2.4 shows a list of slope efficiencies $E_s = \frac{\Delta P}{\Delta I}$ and differential resistances $R_d = \frac{\Delta U}{\Delta I}$ at 6 mA bias current for different temperatures.

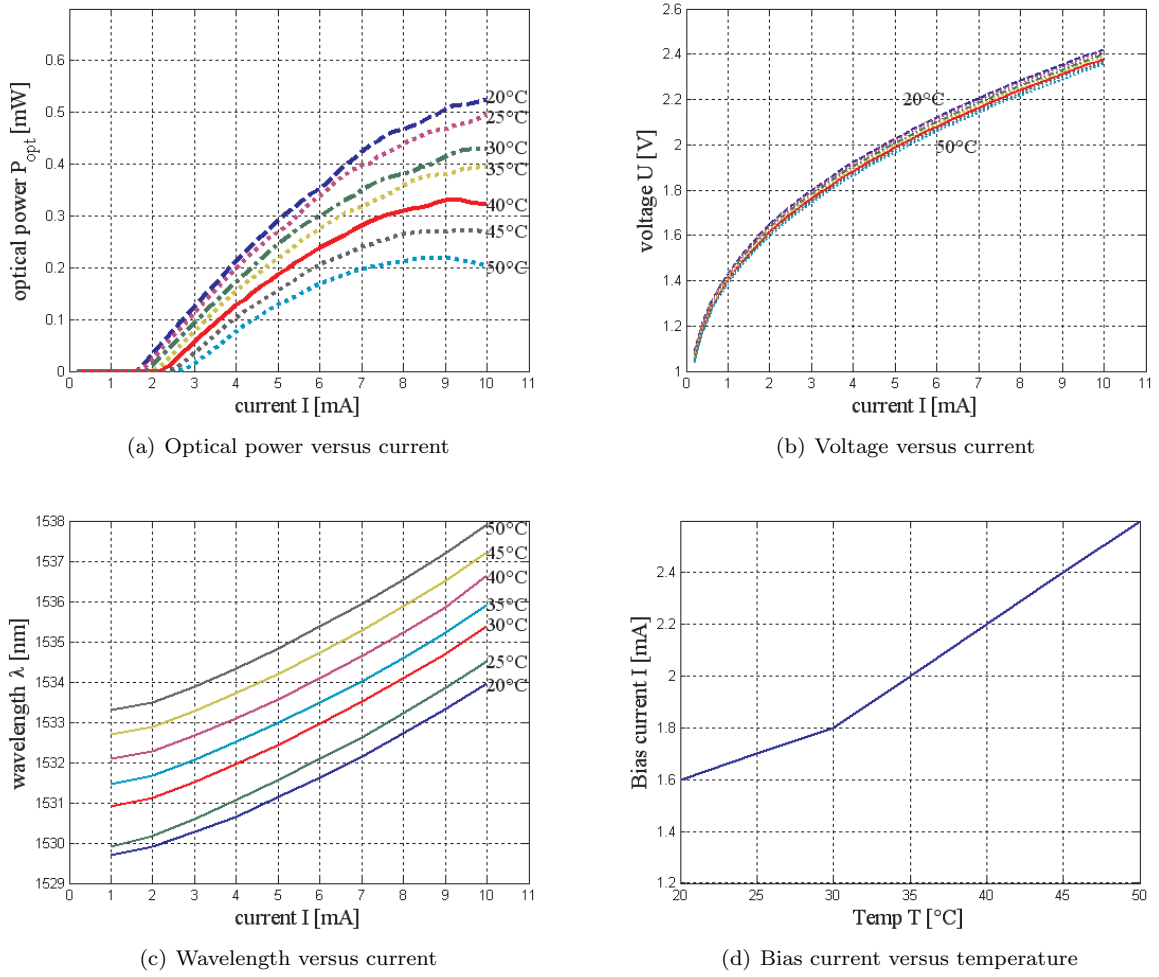


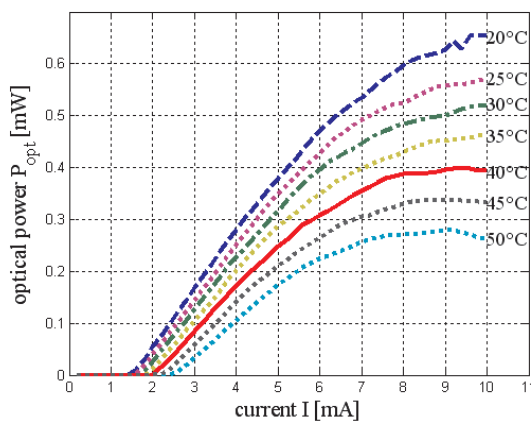
Figure 2.7: Static characteristics at various temperatures of the 1531 nm RayCan VCSEL: a) P-I characteristics, b) U-I characteristics, c) wavelength versus laser current d) threshold current versus temperature.

Temp [°C]	E_s [W/A]	R_d [Ω]
20	0.06608	88.1
25	0.06224	87.7
30	0.05035	87.3
35	0.04895	86.8
40	0.04615	86.3
45	0.03951	85.9
50	0.03216	85.7

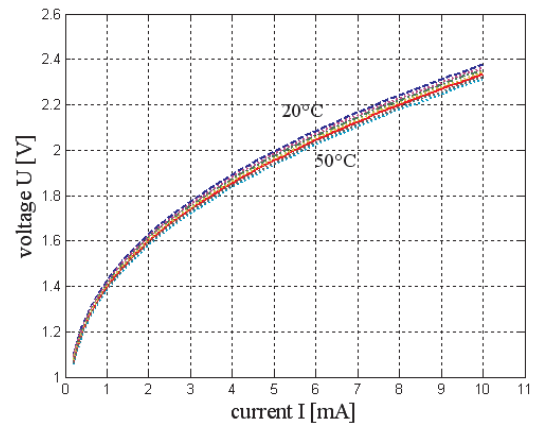
Table 2.4: Slope efficiency E_s and differential resistance R_d of the 1531 nm RayCan VCSEL as a function of the ambient temperature.

Static characteristics of the 1538 nm RayCan VCSEL

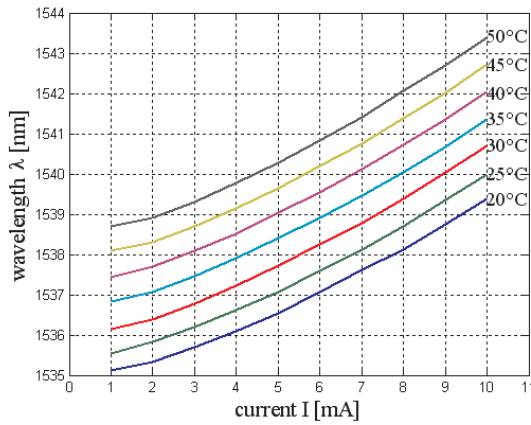
Figure 2.8(a) depicts the optical output power versus the laser current of an 1538nm RayCan VCSEL as a function of the ambient temperature. The 1538nm center wavelength of the laser is very close to the upper edge of the 1531 nm wavelength band, which is at 1541 nm. The covered wavelength range can be seen from Figure 2.8(c) to be from 1535.1 to 1543.4nm which is not entirely within the 1531 nm band. The covered wavelength at the optimum bias current of 6 mA is 1537.1 to 1540.8 nm which again is within the specified 1531 nm band, but still very close to the upper band. The variation of the output power with temperature is $8.7 \mu\text{W/K}$ at a bias current of 6 mA. Figure 2.5(d) shows the threshold current versus ambient temperature corresponding to a shift of 1 mA when changing the temperature from 20°C to 50°C (which can also be observed in Figure 2.8(a)). Table 2.5 shows a list of slope efficiencies $E_s = \frac{\Delta P}{\Delta I}$ and differential resistances $R_d = \frac{\Delta U}{\Delta I}$ at 6 mA bias current for different temperatures.



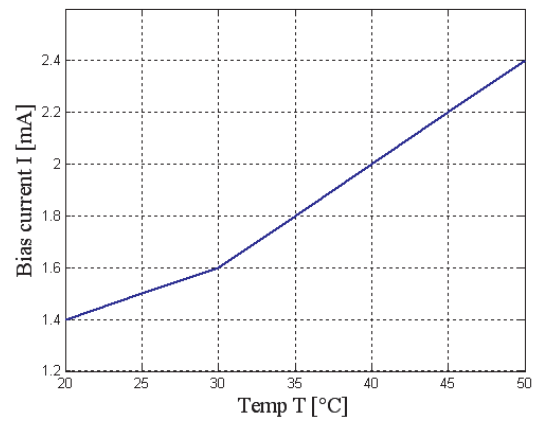
(a) Optical power versus current



(b) Voltage versus current



(c) Wavelength versus current



(d) Bias current versus temperature

Figure 2.8: Static characteristics at various temperatures of the 1538nm RayCan VCSEL: a) P-I characteristics, b) U-I characteristics, c) wavelength versus laser current d) threshold current versus temperature.

Temp [°C]	E_s [W/A]	R_d [Ω]
20	0.07937	84
25	0.06748	83.8
30	0.05804	83.5
35	0.05035	83.2
40	0.04825	82.9
45	0.04615	82.6
50	0.03601	82.4

Table 2.5: Slope efficiency E_s and differential resistance R_d of the 1538 nm RayCan VCSEL as a function of the ambient temperature.

Optical spectra of the RayCan VCSELs

Figure 2.9 displays the spectra of the RayCan VCSELs. The spectra are taken with the optical spectrum analyzer Yokogawa AQ6319 at a bias current of 6 mA and at room temperature $T=25^\circ\text{C}$. The resolution bandwidth of the spectrum analyzer is chosen to be 0.01 nm. The intended single mode spectrum shows a smaller second line approximately 0.5 nm from the main mode in the direction of longer wavelength and 40 dBm below it. Only the spectrum of the 1524 nm VCSEL shows two additional modes at lower wavelengths which were about -60 dBm at their peak values. The lasers are specified as single mode lasers [6] since the side mode suppression ratio (SMSR) which is the ratio between the power level of the dominant line to the next mode in the spectrum is larger than 30 dB. The side modes did not affect the overall performance of the system, and their influence could therefore be neglected.

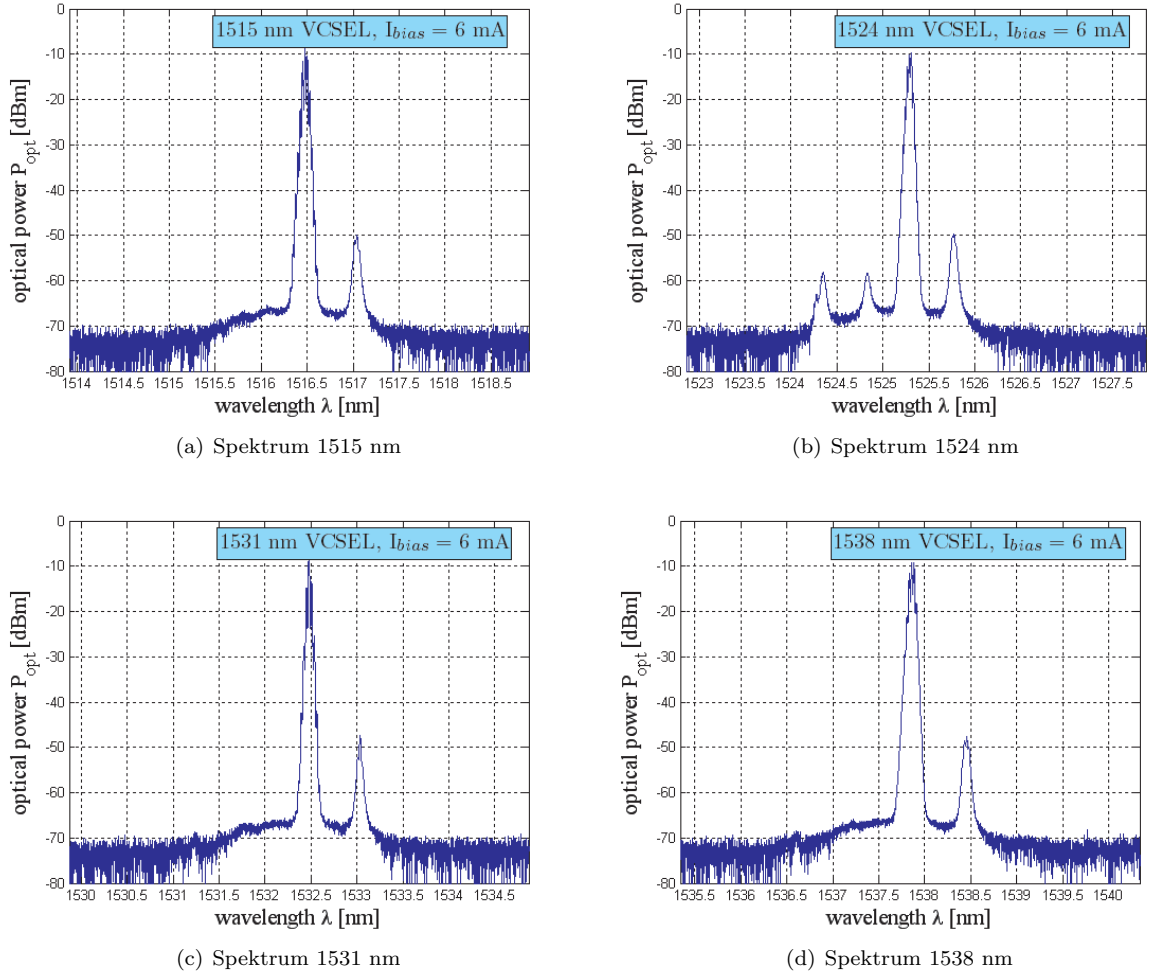


Figure 2.9: Optical spectra of the RayCan VCSELs.

2.1.2 Dynamic properties of the VCSELs

Optical limitation of the RayCan lasers

The Vertilas lasers were limited in their data rate to $R_b = 2.5 \text{ Gb/s}$ and could be modified to work at a data rate of 10.7 Gb/s [4]. In Figure 2.10 the optical modulation response of the 1591 nm Vertilas lasers can be seen. The curves have the characteristic of capacitive loading curves. The rise and fall time of the optical modulation response equals approximately 1 ns which is too slow for a modulation with 10.7 Gb/s . To test the intrinsic rise and fall time of the modulation response, the modulation of the laser is performed at a lower bias current so that the current sometimes drops below the laser threshold. This case can be observed in the right diagram of Figure 2.10 which is a version with a larger time resolution of the left diagram. In this case the rise time of the modulation response was measured to be 40 ps ,

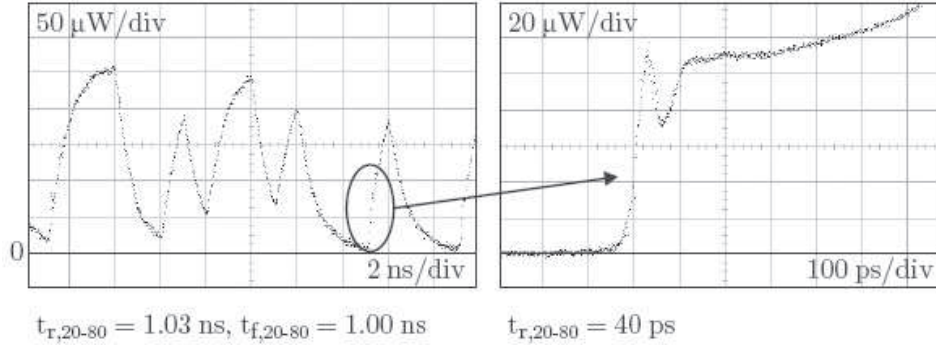


Figure 2.10: Modulation response of the Vertilas 1591 nm VCSEL [4].

which is enough to perform a modulation at 10.7 Gb/s since the duration of one bit $T = \frac{1}{R_b} = \frac{1}{10.7 \text{ Gb/s}} = 93.46 \text{ ns}$ is larger than the sum of rise and fall time. From this result it can be concluded that the capacitive curves were the result of parasitic capacitances leading to the equivalent circuit in Figure 2.11.

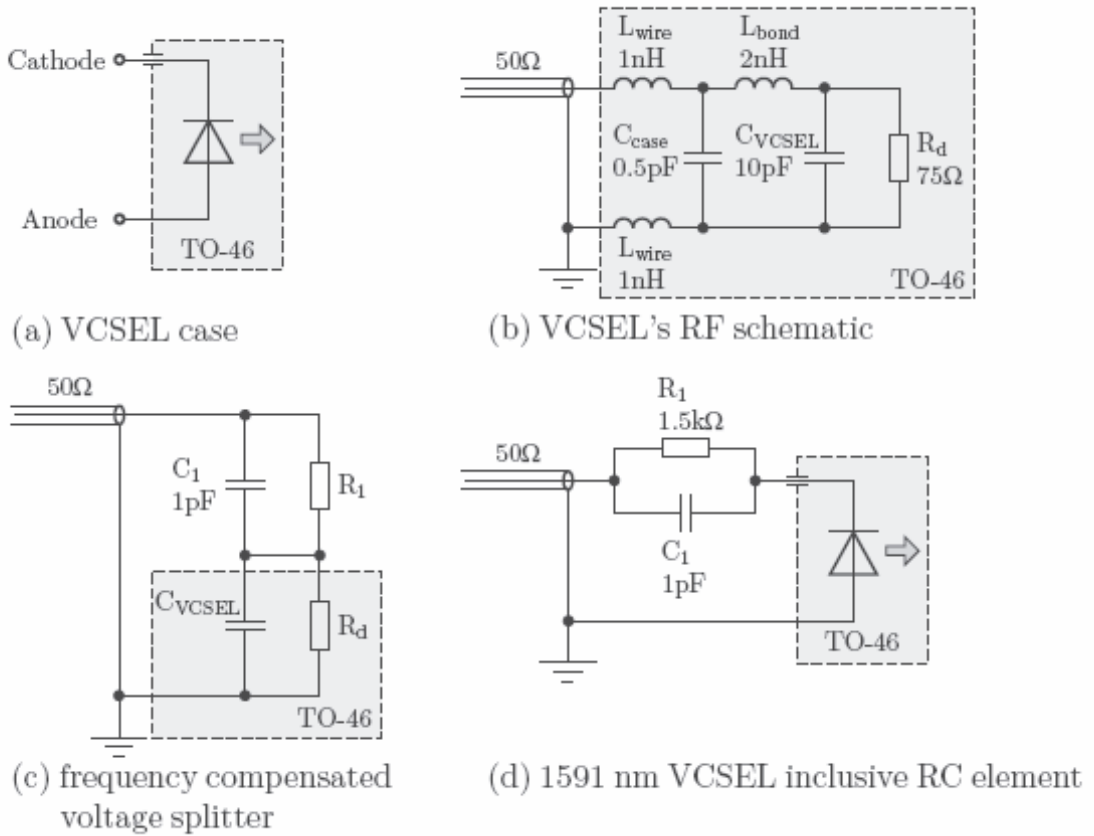


Figure 2.11: Upgrade of the Vertilas 1591 nm VCSEL [4].

The differential resistance R_d is measured in the voltage current curves and the parasitic capacitance C_{VCSEL} is calculated from the time constant $\tau = R_d * C_{VCSEL}$ measured in the optical modulation response. A frequency compensated voltage splitter was used to modify the laser and give a flat response.

modulation response over the whole frequency band. For this purpose the time constants $\tau = R_d * C_{VCSEL}$ and $\tau_1 = R_1 * C_1$ had to be the same. C_1 was chosen such that the time constant of the 50 Ω micro strip line multiplied with C_1 was less than 50 ps to guarantee a 10.7 Gb/s modulation [4]. To avoid further parasitic components the capacitor C_1 and the resistor R_1 were mounted very close to the VCSEL housing as displayed in Figure 2.12(a).

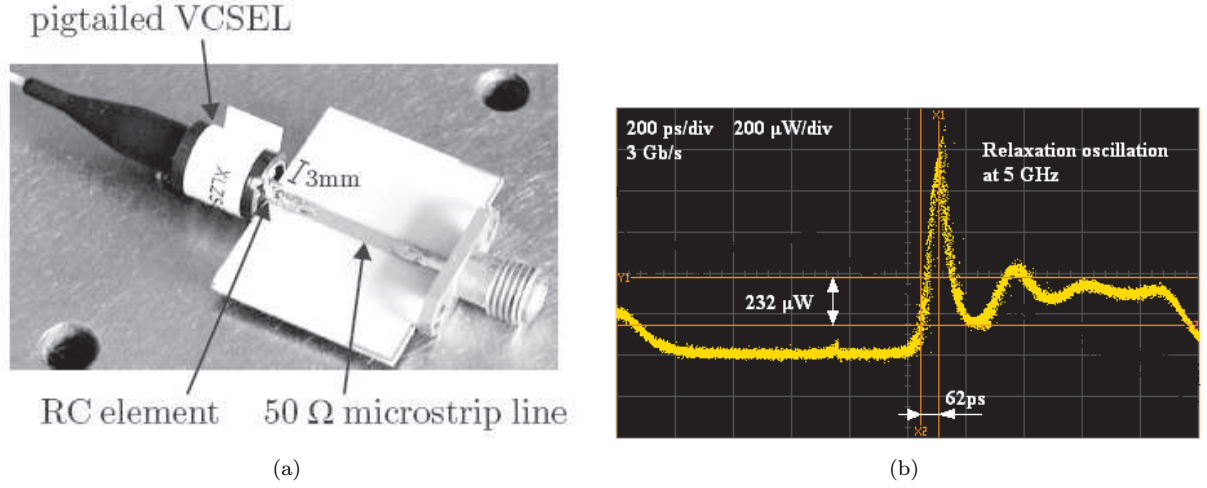


Figure 2.12: a) Photo of the Vertilas VCSEL with RC element [4]. b) Optical modulation response of the 1538 nm RayCan laser with relaxation oscillations.

The modulation response of the 1538 nm RayCan VCSEL is displayed in Figure 2.12(b). The major difference to the Vertilas VCSELs are their larger relaxation oscillations. Despite this difference I have tried to apply the before mentioned method of dimensioning the frequency compensated voltage splitter and also tried to apply several other empirical values for the components but could not achieve the same result. These relaxation oscillations are an optical phenomenon and can't be modified with an external electrical circuit. A way to change the characteristics of the modulation response is the insertion of photo active layers into the laser cavity [12].

2.2 Receivers

As receivers for the system I use PIN- and APD-diodes. APD diodes have a greater sensitivity compared to the PIN diodes and therefore potentially increasing the transmission distance.

2.2.1 APD Diode

I use an APD¹ diode which utilizes the avalanche effect to achieve a higher sensitivity due to photo electron multiplication [13]. The APD in use is a "high sensitivity 10 Gb/s surface mount coplanar APD preamplified receiver" called AT10XGC [14] with a connectorized single-mode fiber pigtail. It provides differential outputs to improve noise rejection for enhanced sensitivity. A picture of the surface mount device (SMD) package can be seen in Figure 2.13(a). The internal schematic consisting of an avalanche photo diode, a low-noise preamplifier, and a precision negative temperature coefficient (NTC) thermistor can be seen in Figure 2.13(b).

¹A data sheet of the APD diode AT10XGC can be found in appendix A

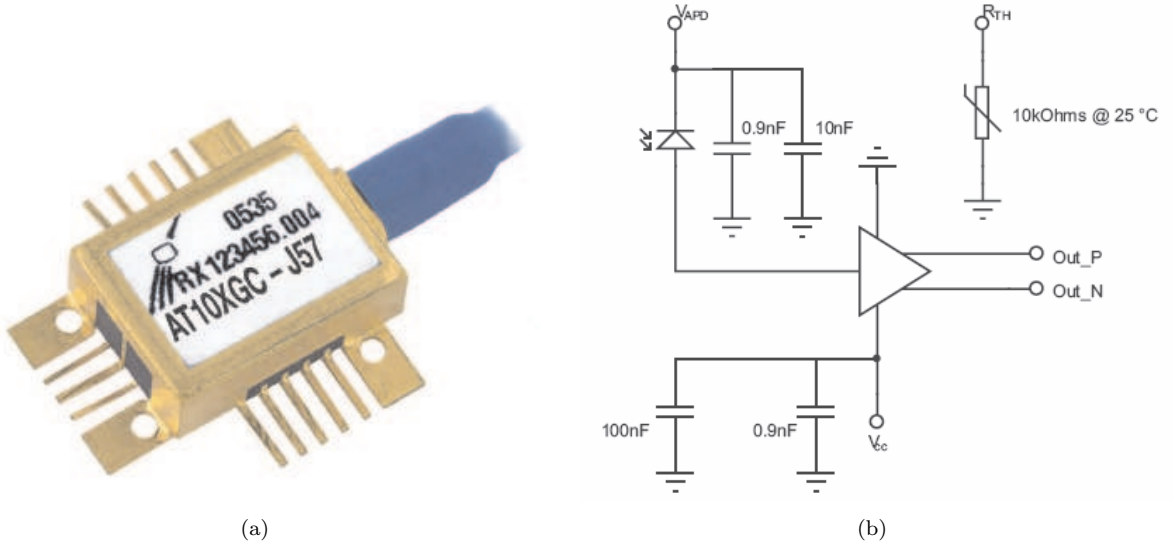


Figure 2.13: The avalanche photo diode AT10XGC: a) SMD housing with single-mode fiber pigtail [14] b) principal internal schematic of the APD [14].

To operate the APD I designed a printed circuit board (PCB) with the software packet EAGLE. The schematic and print layout are shown in Figure 2.14(a) and Figure 2.14(b). Two voltages need to be applied to the AT10XGC integrated circuit (IC) one of 3.3 V to pin 14 for the low-noise preamplifier and one variable voltage to pin 2 as APD bias. The APD bias voltage must be below the breakdown voltage V_{br} which is the maximum voltage that can be applied in blocking direction without damaging the diode. The APD bias voltage must be above the V_{M3} voltage in the presence of a high optical input power to avoid damage of the diode. V_{M3} is the bias voltage at which an electron hole pair generated by one photon is multiplied through the avalanche effect by three so that in this case three electron hole pairs are contributing to the current flow. Analogous is the definition of the V_{M10} voltage with the only difference that the multiplication factor is ten. The V_{M3} and V_{br} voltage are different for each AT10XGC and are provided by the vendor on the fiber tag of each device. The supply voltage of the PCB was chosen to be 33 V. I used a fixed voltage stabilizing IC LM1117MP-3.3 [15] for the 3.3 V supply and a LM317 [16] variable voltage stabilizing IC where the output voltage can be regulated by choosing appropriate resistors. A L7805ACV [17] stabilizing IC is serving as a 5 V supply to the LM1117MP-3.3 3.3 V stabilizing IC, protecting it from the 33 V supply voltage since the maximum input voltage to the LM1117MP-3.3 is only 20 V. The variable voltage on the output pin of the LM317 is determined by

$$U = U_{lo} + \frac{U_{lo}}{R_1} * (R_2 + R_3), \quad (2.1)$$

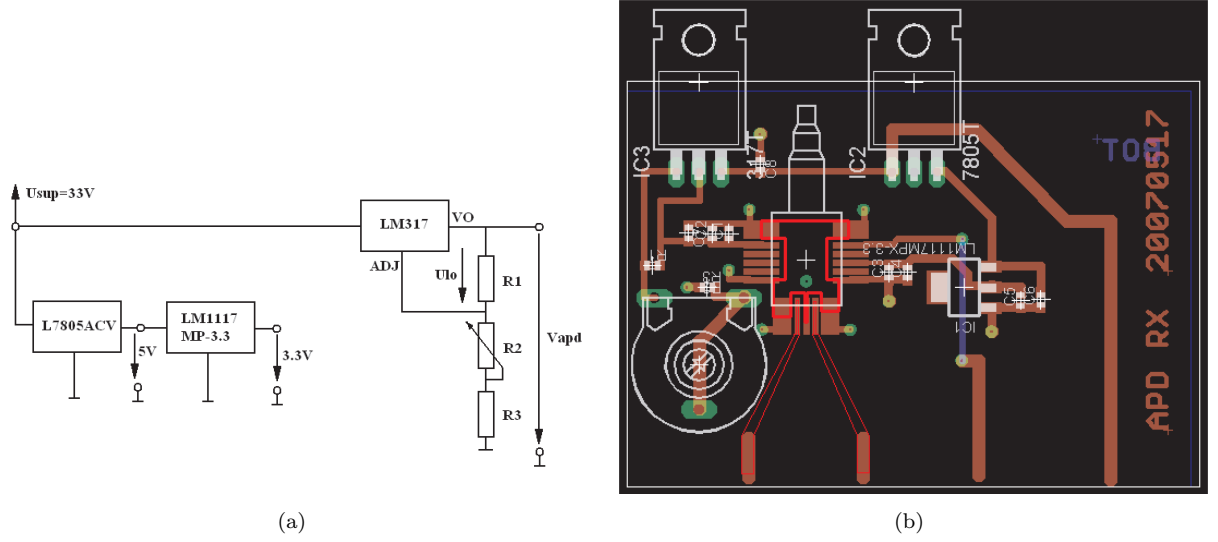


Figure 2.14: a) The circuit for the operation of the APD AT10XGC b) Print layout created with the software package EAGLE.

where U_{lo} is a fixed voltage of 1.25 V between the VO and the ADJ pin across the resistor R1 that defines the current through the voltage divider R1, R2 and R3. The variable resistor R2 is used to adjust the output voltage and R3 defines the lower limit of the output voltage that should be above $V_{M3} = 20.71 V$. From Figure 2.14(b) it can be seen how the two differential outputs Out_P (pin 10) and Out_N (pin 12) were guided to the edge of the PCB via a 50Ω micro strip line that is tapered off toward the output pins of the APD due to problems with the available space. The PCB is assembled into a housing with connectors for the supply voltage of 33 V the APD bias voltage monitoring output and the R_{th} output. For the data outputs Out_P and Out_N I used standard SMA connectors and for the optical data input a FC connector.



Figure 2.15: The fully assembled APD AT10XGC in its housing a) top view b) front view.

The APD voltage for the best BER result i.e. the best receiver sensitivity is determined by the measurement setup in Figure 2.16. The measurement is performed at 10 Gb/s. As optical reference source I use a distributed feedback (DFB) laser [18] which is externally modulated by an electro absorption modulator (EAM). The bias current for the DFB laser is provided by the current source LDC-3724B and equals 60 mA. The EAM is modulated by the BERT's pseudo random bit sequence (PRBS) pattern generator. A PRBS length of $2^{31} - 1$ is used with a modulation voltage of $V_{pp} = 1760 mV$ and an offset voltage of $V_{off} = -775 mV$. A variable optical attenuator is installed between the DFB

laser and the APD diode. The received signal is used by the BER tester of the BERT to calculate the current bit error ratio. A constant attenuation is chosen such that the BERT displays a bit error ratio larger than 10^{-9} , for all measured points, since this is the lowest bit error ratio that can be measured by the BERT.

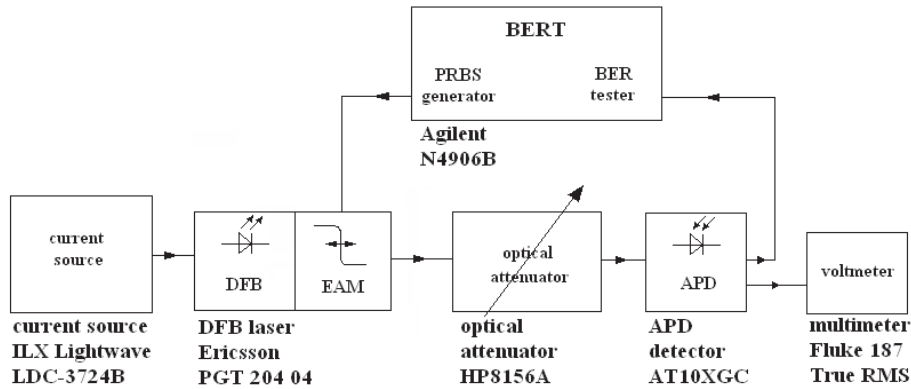


Figure 2.16: Measurement setup for the bit error ratio (BER) versus APD bias voltage measurement.

The APD voltage which is set by the variable resistor R_2 on the PCB is measured by the multimeter Fluke187. The result of this measurement is displayed in Figure 2.17 which shows the BER versus the APD voltage at a bit rate of 10 Gb/s. The optimum APD voltage is found at the minimum bit error rate and equaled 28.42 V.

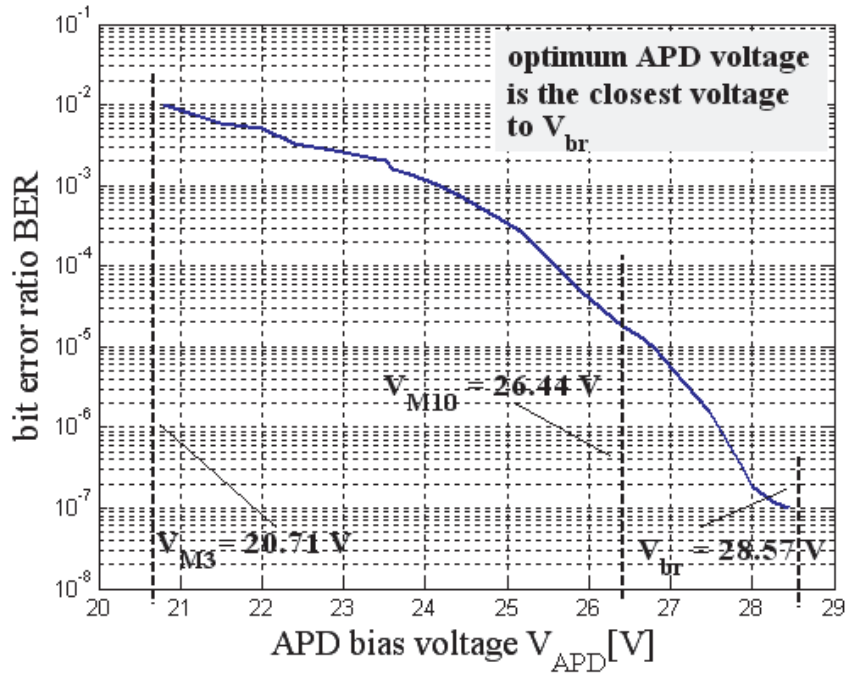


Figure 2.17: Bit error ratio (BER) versus APD bias voltage.

The measurement setup for the back to back (b2b) measurements is shown in Figure 2.18. The bias current for the VCSEL is provided through a bias-tee from the current source Thor Labs PRO800. The pattern generator from the BERT provided the modulation voltage for the VCSEL. The VCSEL's optical output was attenuated by a variable optical attenuator HP8156A and then split by a 3 dB optical power splitter to provide the same signal for the APD diode and the optical power meter Anritsu ML9108 which is used to monitor the optical input power of the APD. The electrical output signal from the APD is fed to the BERT for bit error calculation.

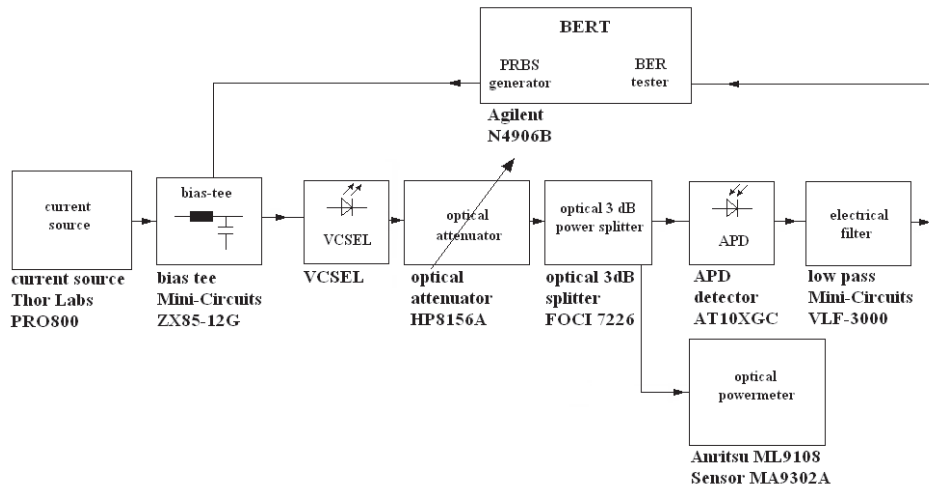


Figure 2.18: Measurement setup for the back to back measurements with VCSELs.

An additional measurement is performed with the external modulated DFB laser to have a reference result. The measurement setup is shown in Figure 2.19.

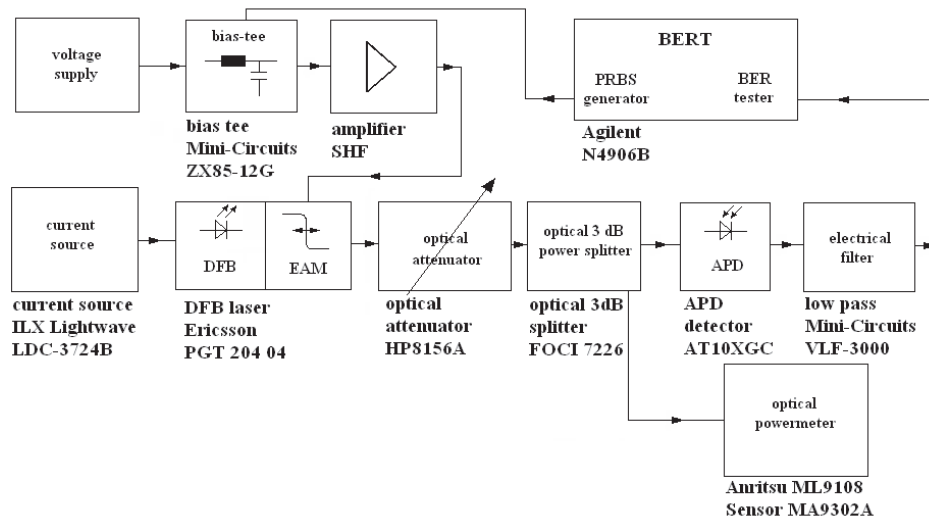


Figure 2.19: Measurement setup for the back to back measurements with DFB laser.

The additional amplifier is used to achieve the maximum modulation swing possible for the EAM with a constant bias of -1 V from the voltage supply. The bit error ratio measurements were performed

with Vertilas, RayCan, and DFB lasers as sources at the data rates of 10.7 Gb/s, 2.5 Gb/s, and 1 Gb/s. A PRBS length of $2^{31} - 1$ is used in the following measurements. The driving conditions, i.e. the modulation swing and bias current, of the lasers is chosen to achieve the best b2b performance. When using a SSMF which adds also dispersion these driving conditions become sub optimum as can be seen in subsequent chapters. Figure 2.20 shows the BER versus the received optical power of the Vertilas VCSELs and the DFB laser at a bit rate of 10.7 Gb/s. The reference curve of the DFB laser shows a BER of 10^{-9} at an optical input power of -26.2 dBm. The best performing VCSEL is the 1551 nm laser which is only 1 dB of the DFB laser reference curve.

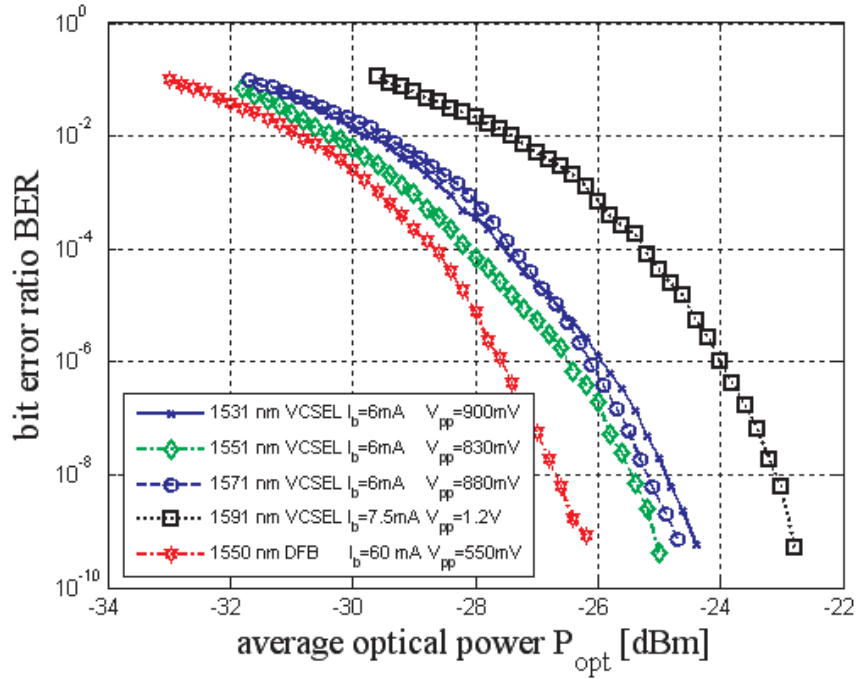


Figure 2.20: BER curves of the Vertilas and the DFB lasers as optical sources and the APD as the optical receiver in back to back configuration at a data rate of 10.7 Gb/s (I_b ...laser bias current, V_{pp} ...modulation swing).

The worst performing laser is the 1591 nm laser with a BER of 10^{-9} at an optical input power of -22.8 dBm. This is due to a lower output power relative to the other VCSELs. The lower output power was caused by an experiment where the 1591 nm VCSEL was heated up to 50°C [4] resulting in a permanent performance degradation. Figure 2.21 shows the BER versus the received optical power of the Vertilas VCSELs and the DFB laser at a bit rate of 1 Gb/s. All lasers performed equally good at a BER of 10^{-9} except the 1591 nm laser which is 0.2 dB worse than the other three Vertilas lasers. The difference to the DFB laser curve equaled to 1 dB. The b2b performance of the Vertilas lasers at 2.5 Gb/s is shown in Figure 2.22. The BER curves of all VCSELs were very close to the ideal curve of the DFB laser with -33.8 dBm at a BER of 10^{-9} .

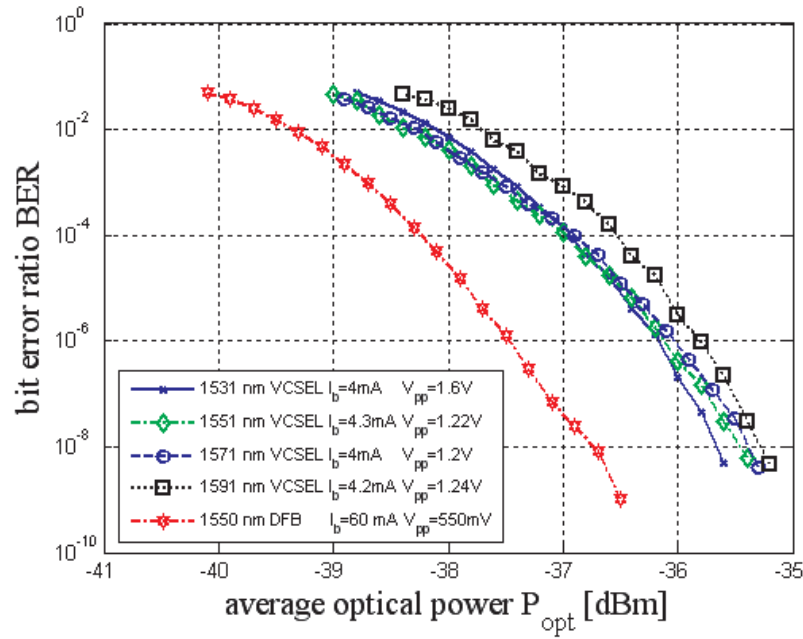


Figure 2.21: BER curves of the Vertilas and the DFB lasers as optical sources and the APD as the optical receiver in back to back configuration at a data rate of 1 Gb/s (I_b ...laser bias current, V_{pp} ...modulation swing).

Figure 2.23 shows the BER versus the average received optical power of the RayCan VCSELs and the DFB laser at a data rate of 1 Gb/s. All four VCSEL curves are equal above a BER of 10^{-5} . Below a BER of 10^{-5} the spacing between the curves was 0.1 dB to 0.2 dB where the 1538 nm VCSEL performed best with a gap of only 0.5 dB relative to the DFB laser. The curves of the RayCan VCSELs and the DFB laser at a data rate of 2.5 Gb/s are shown in Figure 2.24. The 1515 nm and 1538 nm curves are very similar to each other, with the 1538 nm VCSEL performing best with a gap of 1 dB at a BER of 10^{-9} relative to the DFB laser. The worst performance has the 1524 nm VCSEL with a gap of 2 dB when compared to the DFB laser.

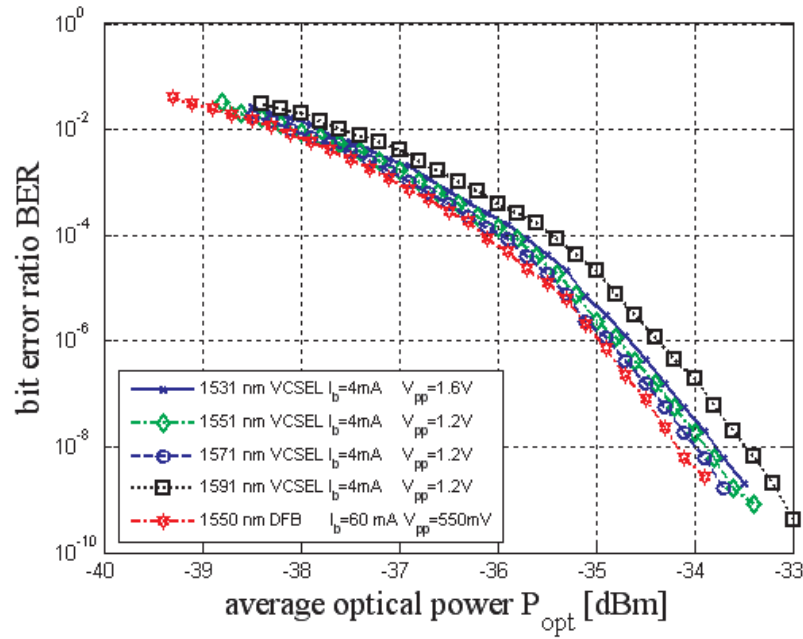


Figure 2.22: BER curves of the Vertilas and the DFB lasers as optical sources and the APD as the optical receiver in back to back configuration at a data rate of 2.5 Gb/s (I_b ...laser bias current, V_{pp} ...modulation swing).

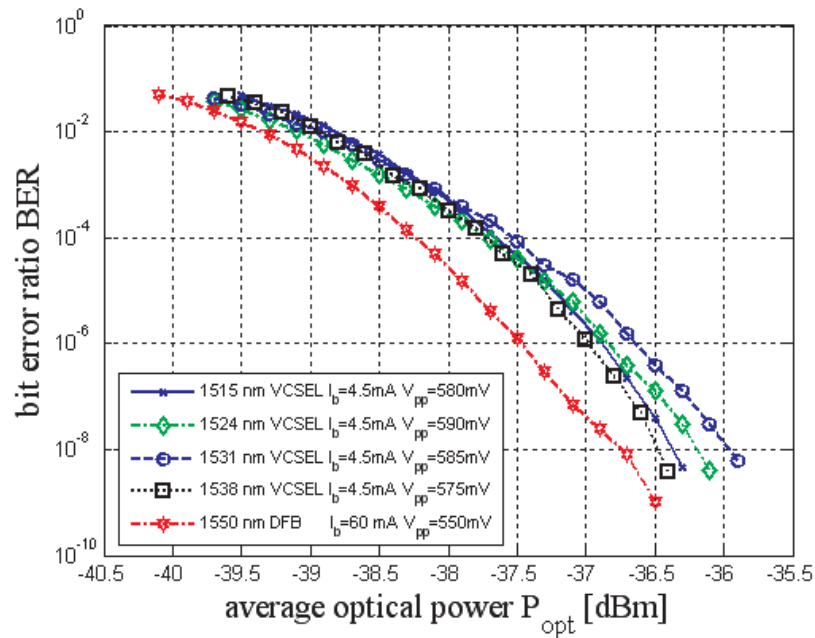


Figure 2.23: BER curves of the RayCan and the DFB lasers as optical sources and the APD as the optical receiver in back to back configuration at a data rate of 1 Gb/s (I_b ...laser bias current, V_{pp} ...modulation swing).

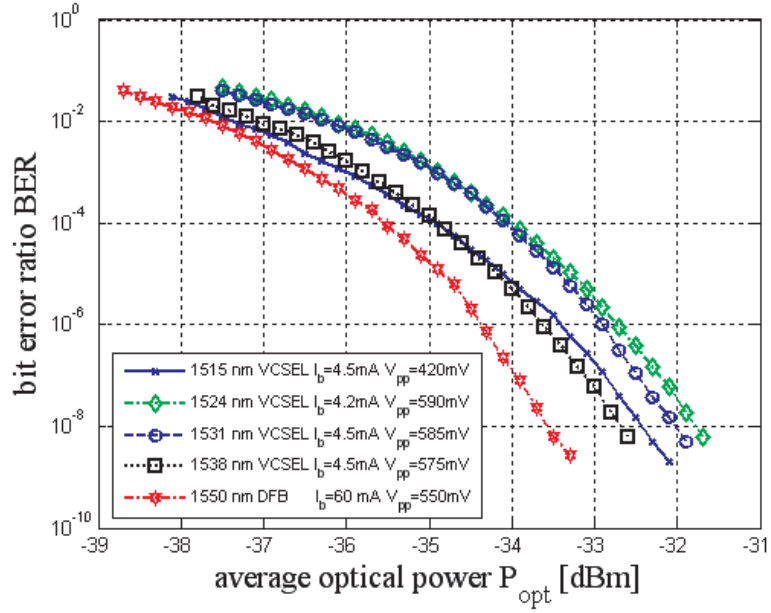


Figure 2.24: BER curves of the RayCan and the DFB lasers as optical sources and the APD as the optical receiver in back to back configuration at a data rate of 2.5 Gb/s (I_b ...laser bias current, V_{pp} ...modulation swing).

2.2.2 PIN Diode

The second receiver type I use is a PIN² diode where measurements at 10.7 Gb/s were already performed [4]. It is a 2860C from Ortel and contained a pin photodiode, a transimpedance amplifier, and a limiting amplifier optimized for a data rate of 10 Gb/s.

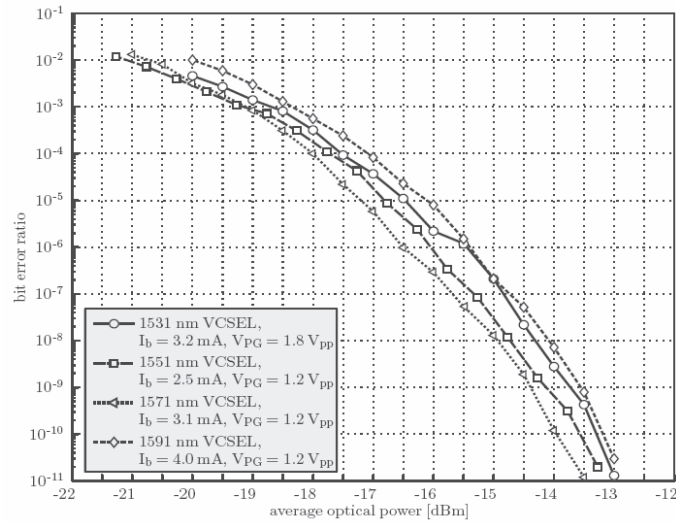


Figure 2.25: BER curves of the Vertilas lasers as optical sources and the PIN as the optical receiver in back to back configuration at a data rate of 10.7 Gb/s [4] (I_b ...laser bias current, V_{PG} ...modulation swing).

²A data sheet of the PIN diode R2860C can be found in appendix A

Figure 2.25 shows the measurement results at a bit rate of 10.7 Gb/s and a PRBS length of $2^{31} - 1$ with the Vertilas VCSELs as sources. Since the measurements for the APD diode have shown that the different lasers do not differ much in terms of BER, I only performed BER measurements for the 1551 nm Vertilas and the 1538 nm RayCan VCSEL and present them as a comparison to the results from the APD measurements in the following section.

2.2.3 Comparison of the performance of the PIN- and APD- Diode

A comparison between the b2b performance of the PIN and the APD diode at 10.7 Gb/s is shown in Figure 2.26. Where the 1551 nm Vertilas VCSEL is used as the optical source. The improvement in the b2b case with APD diode compared to the case with PIN diode equaled 10 dB. For a bit rate of 2.5 Gb/s and 1 Gb/s the measurements were also performed with the 1538 nm RayCan VCSEL. The results for 2.5 Gb/s are shown in Figure 2.27. A gain of 13 dB is achieved in this case. In the case of 1 Gb/s, shown in Figure 2.28, a slightly higher gain of 13.5 dB is possible. This improvement in b2b sensitivity promises better results for the maximum achievable fiber distance with an APD diode than in the case when using an PIN diode.

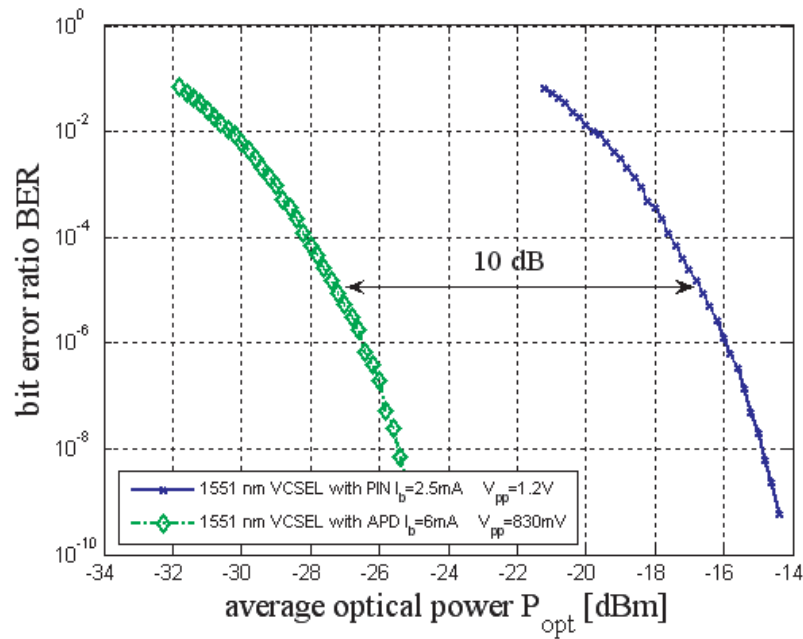


Figure 2.26: Comparison of the BER curves with APD and with PIN diode where the 1551 nm Vertilas VCSEL is used as the optical source at a data rate of 10.7 Gb/s (I_b ...laser bias current, V_{pp} ...modulation swing).

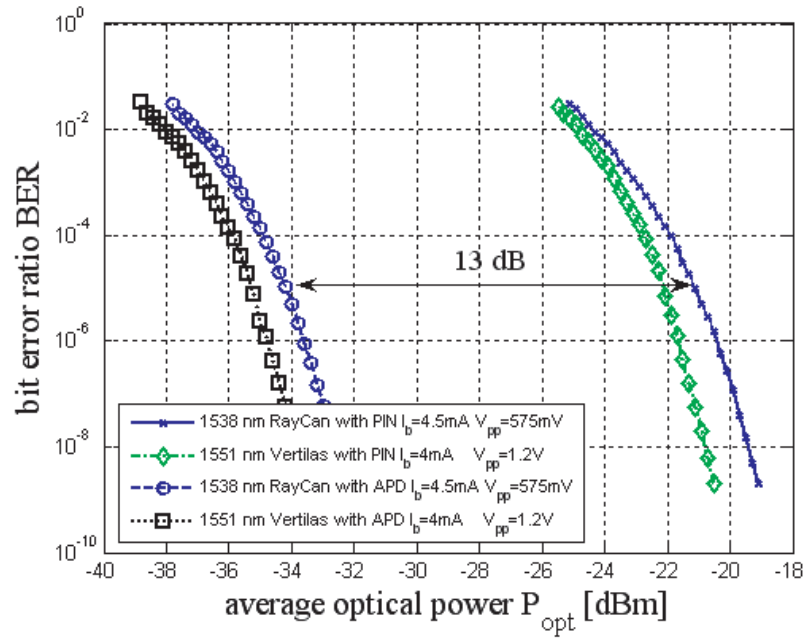


Figure 2.27: Comparison of the BER curves with APD and with PIN diode where the 1551 nm Vertilas and the 1538 nm RayCan VCSELs are used as the optical sources at a data rate of 2.5 Gb/s (I_b ...laser bias current, V_{pp} ...modulation swing).

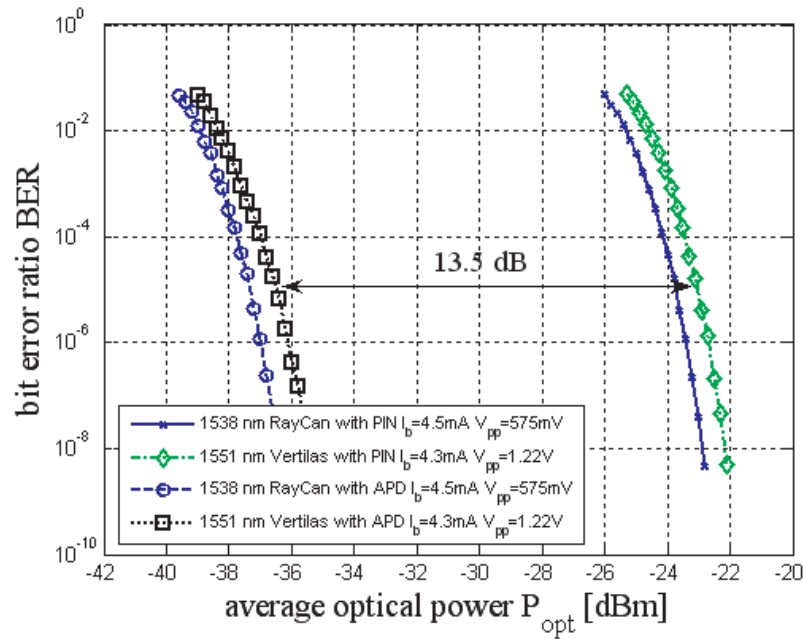


Figure 2.28: Comparison of the BER curves with APD and with PIN diode where the 1551 nm Vertilas and the 1538 nm RayCan VCSELs are used as the optical sources at a data rate of 1 Gb/s (I_b ...laser bias current, V_{pp} ...modulation swing).

2.3 Semiconductor optical amplifier (SOA)

A principal schematic of an SOA³ is shown in Figure 2.29(a). It is built up like a laser diode with the difference that the end faces are coated with an anti reflection layer which prevents oscillations in the active region. The optical signal enters from the left into the SOA and is amplified in the active region through stimulated emission. The amplified signal is coupled out of the SOA on the right side. The SOA is a bidirectional device and can therefore be used in a passive optical network (PON). 3R regeneration is defined as the regeneration of the signals amplitude, pulse shape and timing which is displayed in Figure 2.29(b). An SOA only amplifies the signals amplitude why we speak of an 1R regeneration. In this case the signal is amplified along its distorted pulse shape and its timing jitter which is shown in the middle pulse shape of Figure 2.29(b). This amplified distorted pulse shape may lead to wrongly detected bits at the receiver but is cheaper than 3R regeneration.

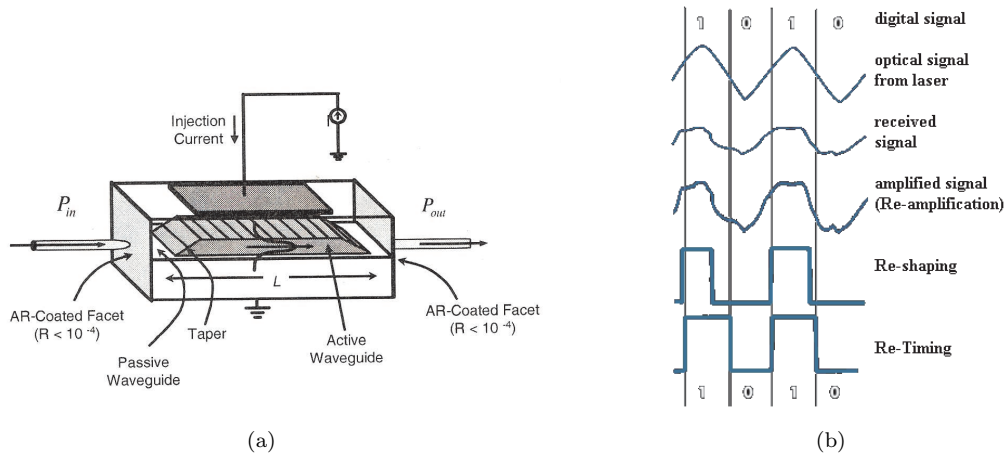


Figure 2.29: a) Principal schematic of the SOA [19] b) 3R regeneration [20].

2.3.1 Static properties of the SOA

The SOA I use is a BOA1004 from Covega [21] which is shown in Figure 2.30. It is controlled by an evaluation board, that is connected through a RS232 interface [22] to a PC. The current and voltage of the SOA is adjusted with the provided evaluation software V-Drive. Temperature control of the SOA can be performed with a built in peltier element. The SOA has an integrated isolator which prevents bidirectional use.

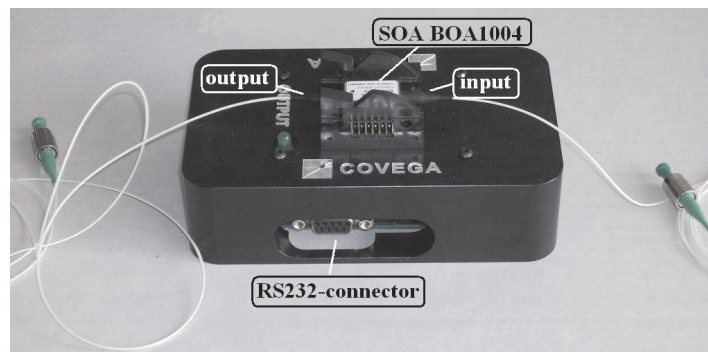


Figure 2.30: Picture of the SOA BOA1004 mounted onto the evaluation board.

³A data sheet of the SOA BOA1004 can be found in appendix A

Figure 2.31 shows the measurement setup for the optical power versus current, voltage versus current and optical spectra measurements. The 1551 nm Vertilas VCSEL is used as laser source, biased at 6 mA by the current source Thor Labs PRO800. The input power into the SOA is regulated through a variable optical attenuator, while the output of the SOA is connected via an optical filter to an optical power meter and to an optical spectrum analyzer.

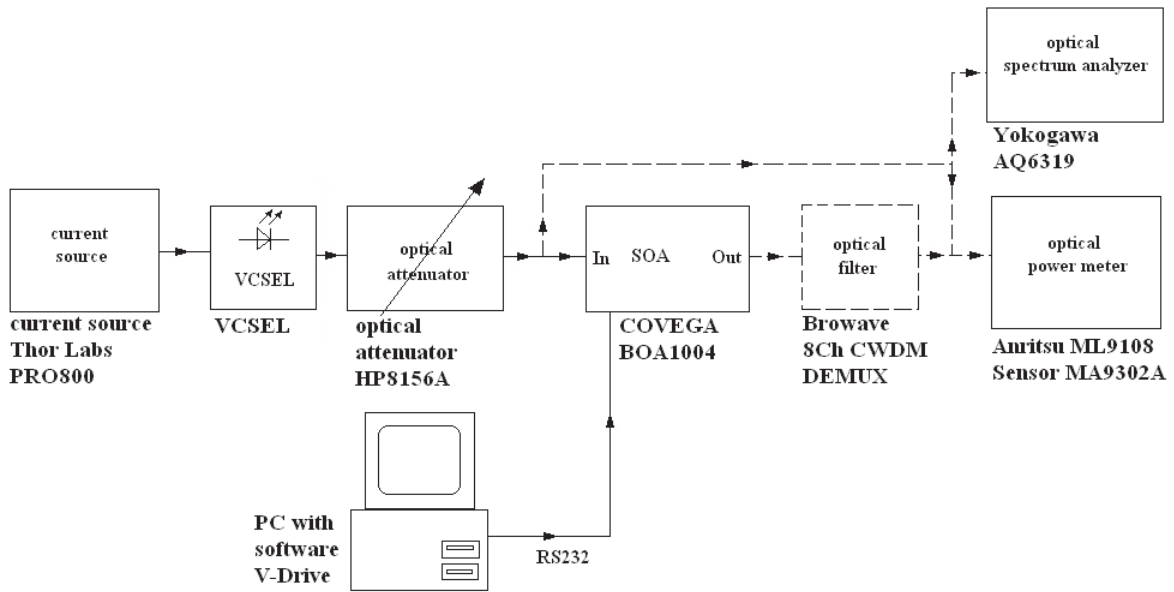


Figure 2.31: Measurement setup for the power versus current, voltage versus current and optical spectra measurements of the SOA BOA1004 from Covega.

Figure 2.32(a) shows the spectrum of the SOA output without optical filter. The measurement is done with a resolution bandwidth (RB) of 0.1 nm. A strong optical power at the output without any input power is caused by the amplified spontaneous emission (ASE) generated within the active region of the SOA. The curve follows the gain of the SOA versus the wavelength [23], the maximum is found at 1525 nm. The ASE spectrum of the SOA is filtered with the 1551 nm filter of the CWDM multiplexer as shown in Figure 2.32(b). It filters a great amount of ASE noise and leaves only the noise within the filters pass band from 1541 to 1561 nm.

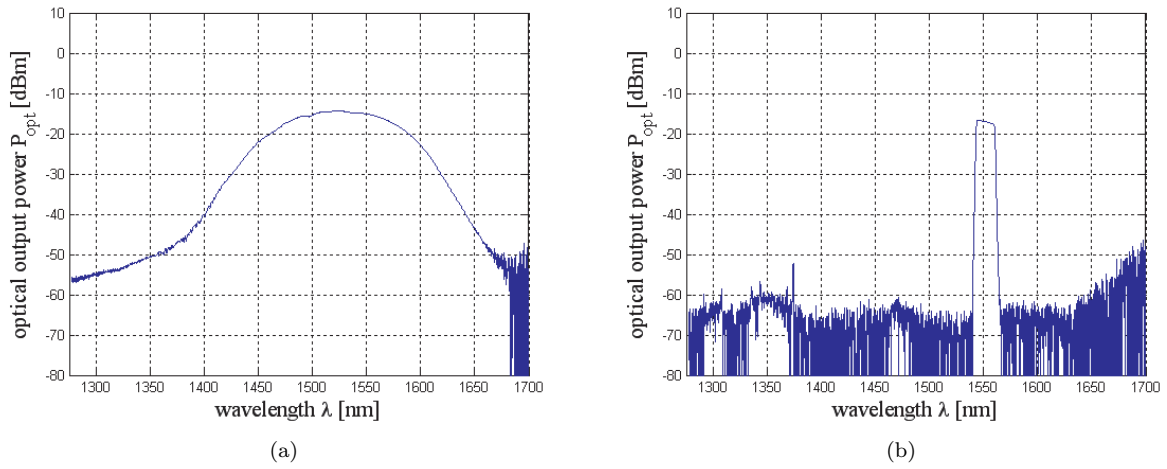


Figure 2.32: Output spectrum of the SOA BOA1004 a) without optical filter b) with optical filter.

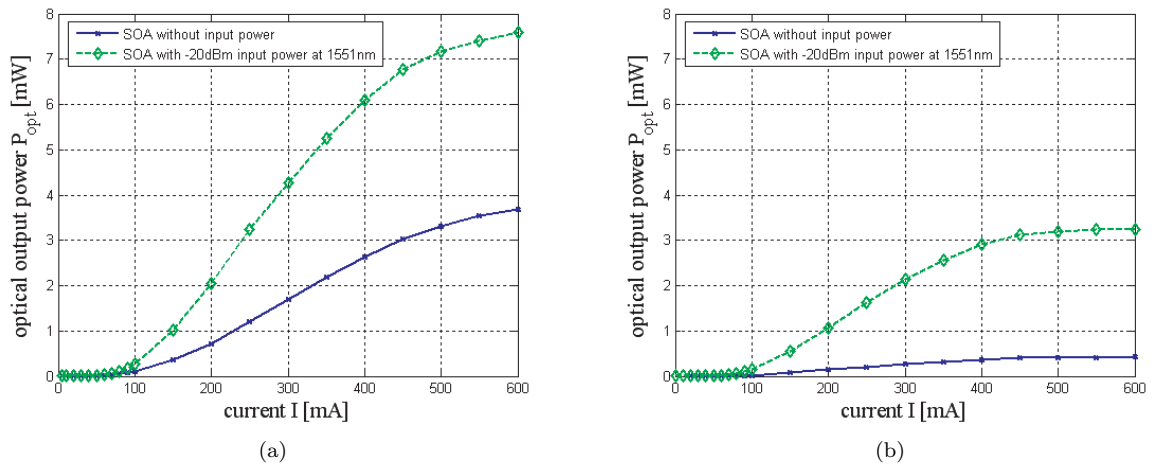


Figure 2.33: Output power versus current of the SOA BOA1004 a) without optical Filter b) with optical Filter.

Figure 2.33 shows the power versus current plots of the SOA, without any input power and with -20 dBm input power, at a wavelength of 1551 nm. The measurement is performed with the wide band optical sensor MA9302A whose wavelength measurement range reaches from 750 nm to 1800 nm. The optical output power increases with increasing SOA current and with increasing input power. A high optical output power of 3.7 mW at 600 mA which is bad for the system performance can be observed in subsequent measurements. With an optical input power of -20 dBm the output power increases to 7.6 mW at 600 mA. The high ASE output power from the SOA can be reduced with an optical filter. Corresponding power versus current plots are shown in Figure 2.33(b). The output power generated by the ASE noise at 600 mA dropped from 3.7 mW without the filter to 0.45 mW with filter.

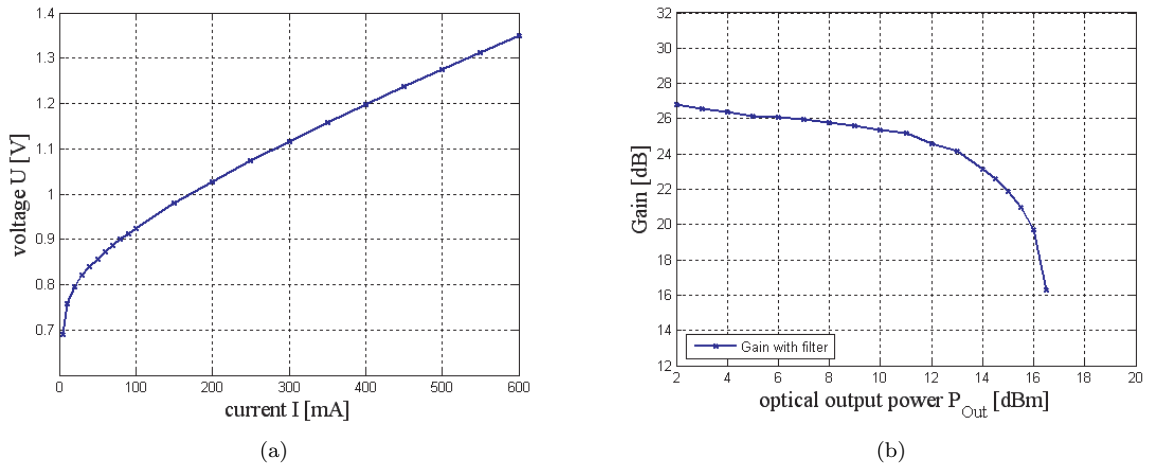


Figure 2.34: a) Voltage versus current of the SOA BOA1004 b) Gain versus optical output power of the SOA.

A plot of the voltage versus the current of the SOA is shown in Figure 2.34(a). A simple diode characteristic can be observed with a forward voltage of 0.7 to 0.8 V. The electrical characteristics of the SOA do not depend on any parameter. The gain of the SOA versus the output power is shown in Figure 2.34(b). One measurement is performed with and one without an optical filter. A gain of up to 26 dB can be achieved in the case with optical filter. The -3 dB point is found at an output power of 14 dBm.

2.3.2 Dynamic properties of the SOA

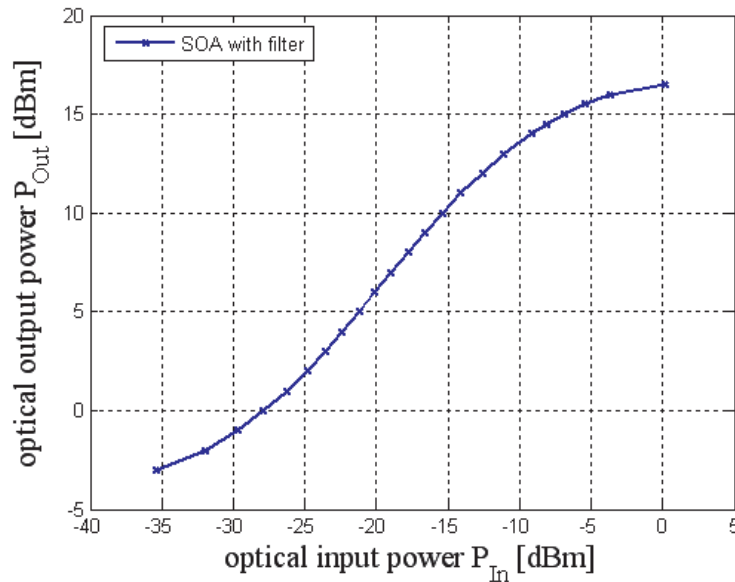


Figure 2.35: Output power versus input power of the SOA BOA1004 from Covega.

A plot of the output power versus the input power is shown in Figure 2.35. From the curve taken with the optical filter it can be seen that the linear region is between -25 and -10 dBm. The eye diagrams

from Figure 2.36 are showing the optical output of the SOA at different input powers. From a) through f) -4 dBm, -6 dBm, -8 dBm, -10 dBm, -12 dBm and -14 dBm. For a higher optical input power of -4 dBm as in Figure 2.36(a) the eye is almost closed, dominated by edge overshoots, indicating deep SOA saturation. The extinction ratio is also degraded at high input powers as the high power “1” experiences strong saturation, the “0”, which is approximately 10 dB lower in power, still experiences nearly the full gain from the SOA. For a lower optical input power of -14 dBm as in Figure 2.36(f) the eye opening decreases due to the lower input power and therefore lower amplification. The best result for the eye diagram in terms of eye opening is found at -12 dBm input power as can be seen from Figure 2.36(e).

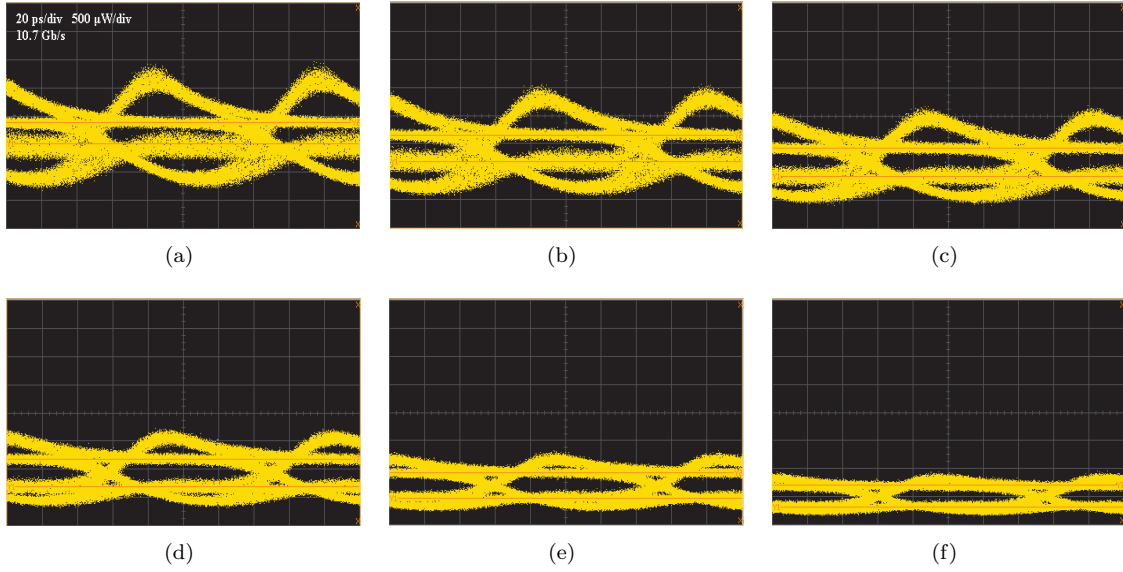


Figure 2.36: Eye diagrams from the SOA output for different input levels a) -4 dBm, b) -6 dBm, c) -8 dBm, d) -10 dBm, e) -12 dBm and f) -14 dBm.

To determine the maximum transmission distance with the SOA in single channel operation I use the measurement setup shown in Figure 2.37. The current source supplies the VCSEL via a bias tee. The BERT modulates the VCSEL with different PRBS lengths. The modulated optical signal is attenuated to be at the optimum -12 dBm input power into the SOA where it gets amplified and transmitted over the SSMF. The optical signal is detected with the APD and the BERT performs the bit error detection. The maximum transmission distance to achieve a certain BER is noted in Table 2.6 along with the used PRBS length. These measurements are performed with and without the SOA and the result is that the performance with SOA is worse than without. This is due to the large amount of ASE at the output of the SOA. I also tried to replace the optical attenuator by an SSMF and by that use the SOA as an inline amplifier, but as expected dispersion of the SSMF lead to a even more distorted amplified signal after the SOA. This makes it impossible to get a BER below 10^{-3} even for shorter distances than those achieved in Table 2.6.

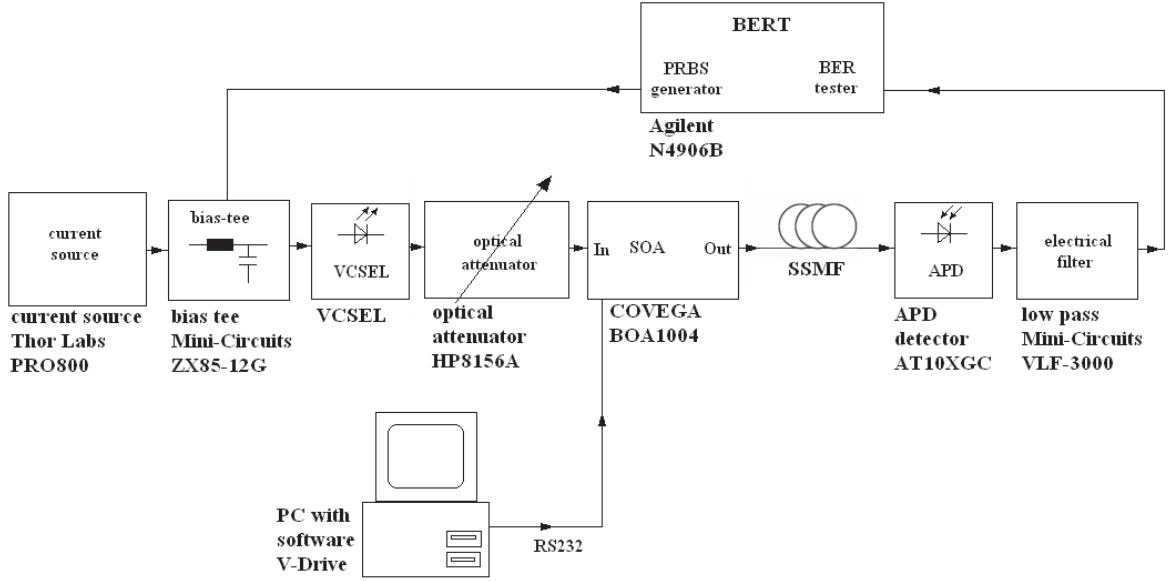


Figure 2.37: Measurement setup for the determination of the maximum fiber distance.

PRBS	BER	with SOA	without SOA
$2^{31} - 1$	10^{-9}	15 km	20 km
$2^7 - 1$	10^{-9}	45 km	55 km
$2^{31} - 1$	10^{-3}	55km	65 km
$2^7 - 1$	10^{-3}	77 km	87 km

Table 2.6: Achieved transmission distances with and without the SOA for different BERs and PRBS lengths.

2.4 Multiplexer and demultiplexer

The desired properties of a CWDM multiplexing/demultiplexing filter are a low insertion loss and a flat passband characteristic for the possible wide wavelength variation of the transmitting lasers. Low cost and compact design are also desired. These properties are already embodied in thin film technology, which is a well known inexpensive and easy to handle process. Thin film filters (TFF's) can be designed with a flat spectral response combined with a low insertion loss. The technology uses thin layers of dielectric material of different refraction index to build wavelength dependent wave guides with passband character [23]. The 8-channel multiplexing (MUX) and demultiplexing (DEMUX) filters used in the CWDM system are purchased from Browave Corporation [24]. The measurement setup in Figure 2.38 is used to retain the spectral characteristics of the MUX and the DEMUX. A white light source is used as the input and the insertion loss is measured with the spectrum analyzer. Figure 2.39 depicts the transmission characteristics of the multiplexing and demultiplexing filters. Table 2.7 lists the insertion losses for the multiplexer and the demultiplexer at the VCSELs emission wavelengths.

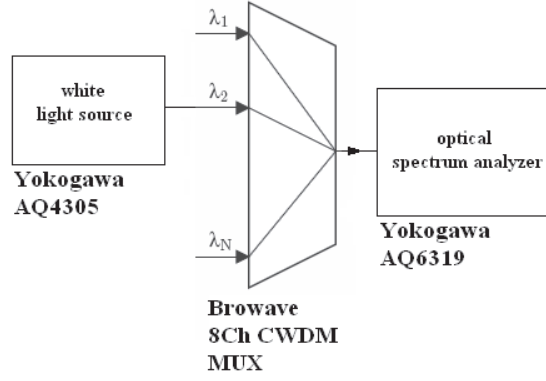


Figure 2.38: Measurement setup for the spectral characterization of the multiplexer MUX and the demultiplexer DEMUX.

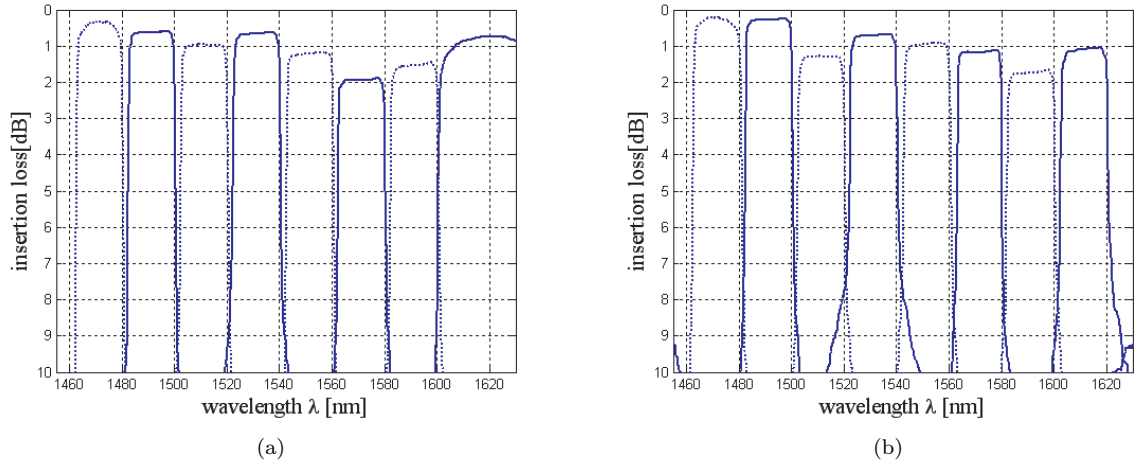


Figure 2.39: The spectral characteristics of the a) multiplexer MUX and b) demultiplexer DEMUX.

Laser	emission wavelength	multiplexer	demultiplexer
RayCan 1515 nm	1516.5 nm	0.9765 dB	1.298 dB
RayCan 1524 nm	1525.3 nm	0.6895 dB	0.74 dB
RayCan 1531 nm	1532.5 nm	0.652 dB	0.7015 dB
RayCan 1538 nm	1537.8 nm	0.62 dB	0.6715 dB
Vertilas 1531 nm	1530.1 nm	0.6685 dB	0.72 dB
Vertilas 1551 nm	1548.7 nm	1.2445 dB	0.9785 dB
Vertilas 1571 nm	1569.8 nm	1.953 dB	1.1835 dB
Vertilas 1591 nm	1589.2 nm	1.548 dB	1.748 dB

Table 2.7: Insertion losses of the CWDM multiplexer and demultiplexer listed for the emission wavelengths of the VCSELs at room temperature 25 °C.

2.5 Optical 3 dB splitter

In the optical 3 dB splitter from FOCI [25] 49.2 % of the input power is directed to the output F00 and 50.8 % to the other output P3 measured at a wavelength of 1551 nm. Figure 2.40 shows the measurement setup for the spectral characterisation of the 3 dB splitter. A white light source is used at the input of the 3 dB splitter. The spectrum at the output of the 3 dB splitter is measured with the optical spectrum analyzer in the wavelength band of interest from 1450 nm to 1630 nm.

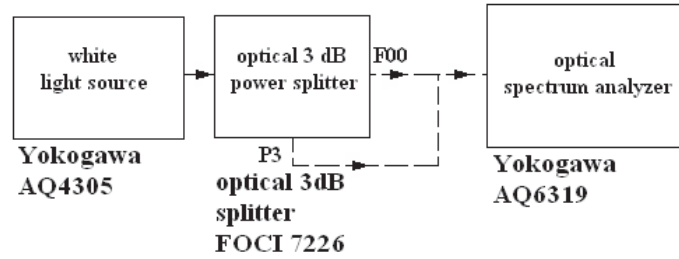


Figure 2.40: Measurement setup for the spectral characterization.

Figure 2.41 shows the insertion loss of the 3 dB splitter. The insertion loss of the output P3 is around 6.5 dB in the measured wavelength area. Output F00 has an decreasing insertion loss from 6 dB at 1450 nm to 5 dB at 1580 nm. In the area above 1580 nm the insertion loss drops below 4 dB.

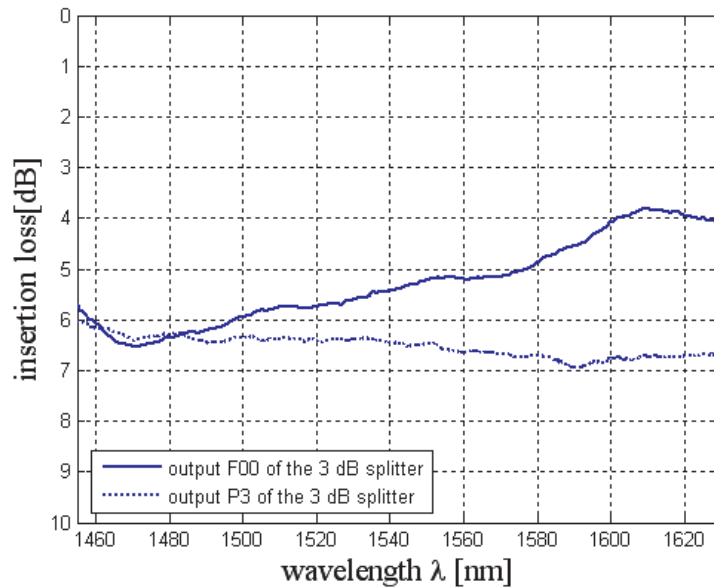
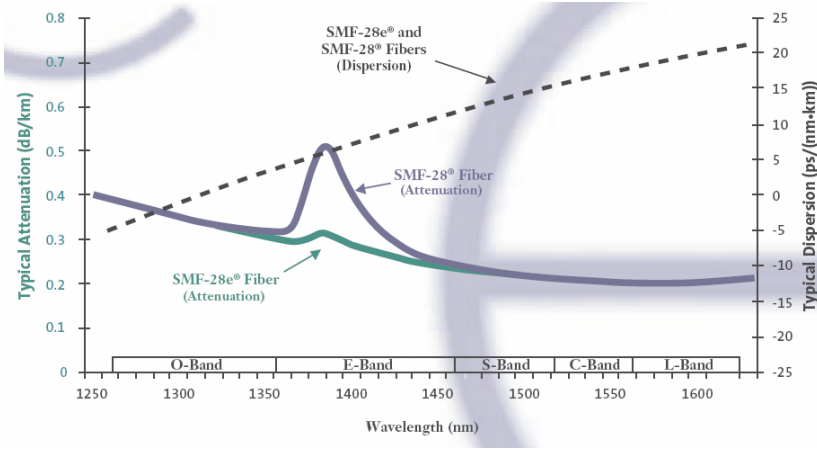


Figure 2.41: Spectral characteristics of the 3 dB splitter in the wavelength range of interest from 1450 nm to 1630 nm.

2.6 Standard single mode fiber

For the SSMF I used already prepared spools of different length listed in Table 2.8. The fiber in use is a SMF-28 from Corning. Figure 2.42(a) shows the attenuation profile and the dispersion versus the wavelength. A picture of the spools is shown in Figure 2.42(b).



(a)



(b)

Figure 2.42: Standard single mode fiber a) attenuation and dispersion profile [26] and b) picture of a spool.

spool	length	attenuation		
		coefficient	measured	calculated
No.1	1.1241 km	0.221 dB/km	0.78 dB	0.2484 dB
No.2	2.1525 km	0.22 dB/km	1.08 dB	0.4735 dB
No.3	5.0208 km	0.213 dB/km	1.39 dB	1.0694 dB
No.4	10.787 km	0.224 dB/km	2.81 dB	2.4162 dB
No.5	14.167 km	0.213 dB/km	3.48 dB	3.0175 dB
No.6	25.640 km	0.22 dB/km	5.87 dB	5.6408 dB
No.7	51.431 km	0.22 dB/km	11.86 dB	11.3148 dB
No.8	77.200 km	0.22 dB/km	17.69 dB	16.984 dB

Table 2.8: Characteristics of the used SSMFs at 1550 nm.

Chapter 3

CWDM system performance

In the previous chapter, I described the characteristics of the components used in the CWDM system, and showed the negative influence of the SOA on the system performance. Effects leading to signal degradation like loss and dispersion were explained, and the possibility of forward error correction for performance enhancement was outlined. In this chapter, I present a comparison of the performance of the system with an PIN diode and an APD diode as the optical receiver. This is done in a single channel as well as a multiple channel operation setup. In the last section I show the transmission of a HD-SDI video signal at a bit rate of 1.485 Gb/s over the system.

3.1 Single channel performance

This section shows the results of single channel transmission over SSMF at a bit rate of 10.7 Gb/s, 2.5 Gb/s and 1 Gb/s using Vertilas and RayCan VCSELs as light sources as well as DFB lasers for a comparison.

3.1.1 System setup for the single channel measurements

Figure 3.1 shows the measurement setup for the single channel performance measurement. The VCSELs were biased and modulated via a bias tee by a current source and the PRBS generator of the BERT. The APD is used as the detector. The SSMF used for the transmission consists of the spools shown in chapter 2.6. To achieve a certain fiber length the spools were connected via APC connectors. These connectors introduce an additional loss which is minimized by connecting not more than three spools together at once. The attenuator is used to be able to control the the received power.

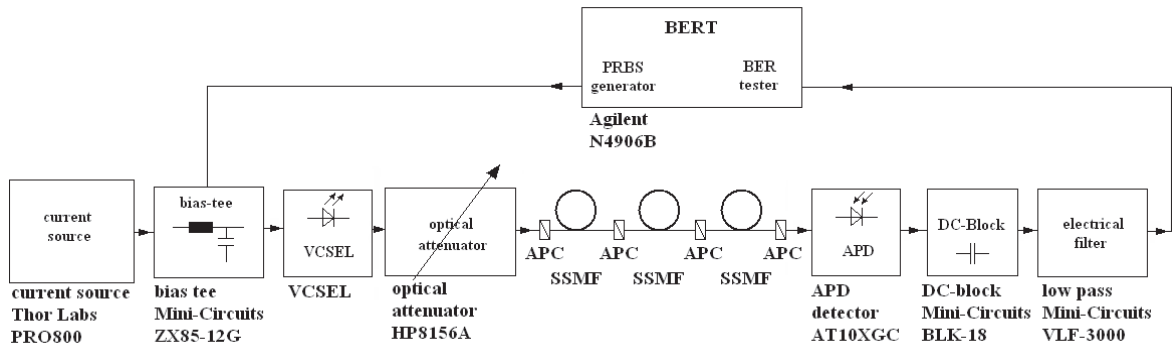


Figure 3.1: Setup for the single channel measurements.

3.1.2 Measurement results at 10.7 Gb/s

Figure 3.2 shows a plot of the minimum required receive power, to achieve a certain BER, versus the fiber length for the Vertilas 1551 nm VCSEL as the source and an APD as the receiver at a bit rate of 10.7 Gb/s. The average output power of the 1551 nm Vertilas VCSEL equals 0.15 dBm. To achieve a BER of 10^{-9} for transmission without FEC and a BER of 10^{-3} for transmission with FEC the decision threshold and the sampling time were optimized manually. The driving conditions of the laser were optimized for maximum reach and are different from those in the b2b case. In the measurements I observed a strong pattern dependence. The upper two curves are taken at a BER of 10^{-9} . The achieved transmission distance of 27 km with a PRBS of $2^{31} - 1$ is less than half of the transmission distance achieved at a PRBS of $2^7 - 1$ which equaled 58 km. This strong pattern dependency favours the use of coding schemes which prevent long runs of ones or zeros which could be a cheaper alternative compared to FEC based transmission. The two lower curves correspond to a BER of 10^{-3} where an FEC implementation can recover the BER to better than 10^{-15} resulting in an increased transmission distance. The difference in transmission distance between a PRBS of $2^{31} - 1$ and $2^7 - 1$ is lower in this case, corresponding to a length of 71 km and 88 km respectively. The s-shape of the curves is due to self phase modulation [4], i.e. the so-called self-steepening effect, which is caused by the chirp of the laser and the dispersion of the SSMF.

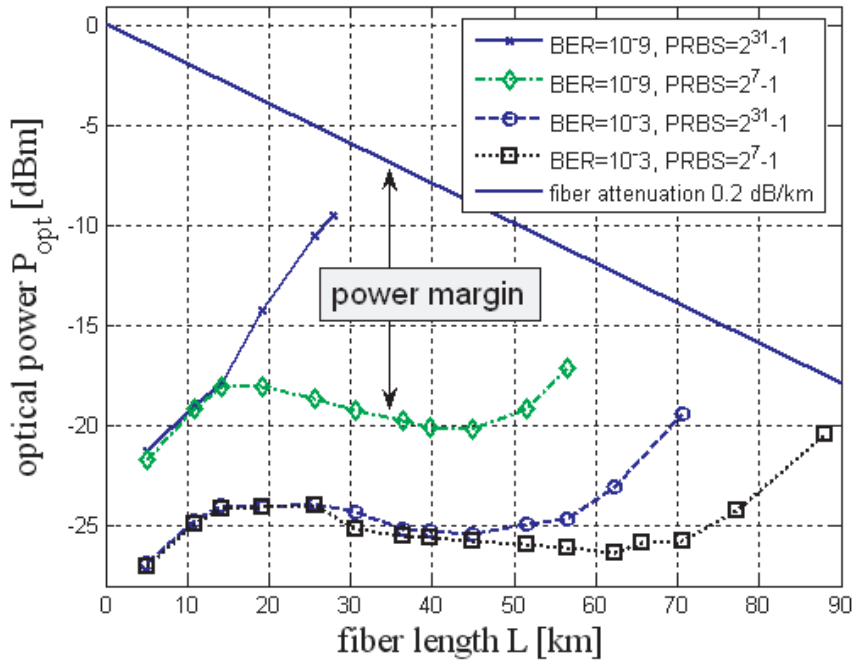


Figure 3.2: Minimum receiver input power versus transmission distance for the 1551 nm Vertilas VCSEL with APD as receiver at a bit rate of 10.7 Gb/s.

Figure 3.3 [4] displays the performance when using a PIN diode as the receiver. Curve c) shows the measurement for a BER of 10^{-9} and PRBS of $2^{31} - 1$ to achieve a maximum distance of 19.2 km while the achieved distance with an APD equaled to 27 km. Due to the strong pattern dependence in the case of the APD a maximum reach of 58 km is achievable without the use of FEC but with the use of a coding scheme which prevents long runs of ones or zeros. For the PIN diode, curve a) shows the results at a BER of 10^{-3} and PRBS of $2^{31} - 1$, the maximum power-limited reach is found to be 65.6 km. The achieved distance with the use of an APD equals to 71 km, which is only achieved with the help of an Erbium doped fiber amplifier (EDFA) curve b) in the case of a PIN diode. Even a distance of 88 km

is achievable when using a PRBS of $2^7 - 1$ with the APD as the receiver. Curves d) and e) show the performance when using the driving conditions for optimum b2b performance of the VCSEL which are sub optimum for a transmission over SSMF.

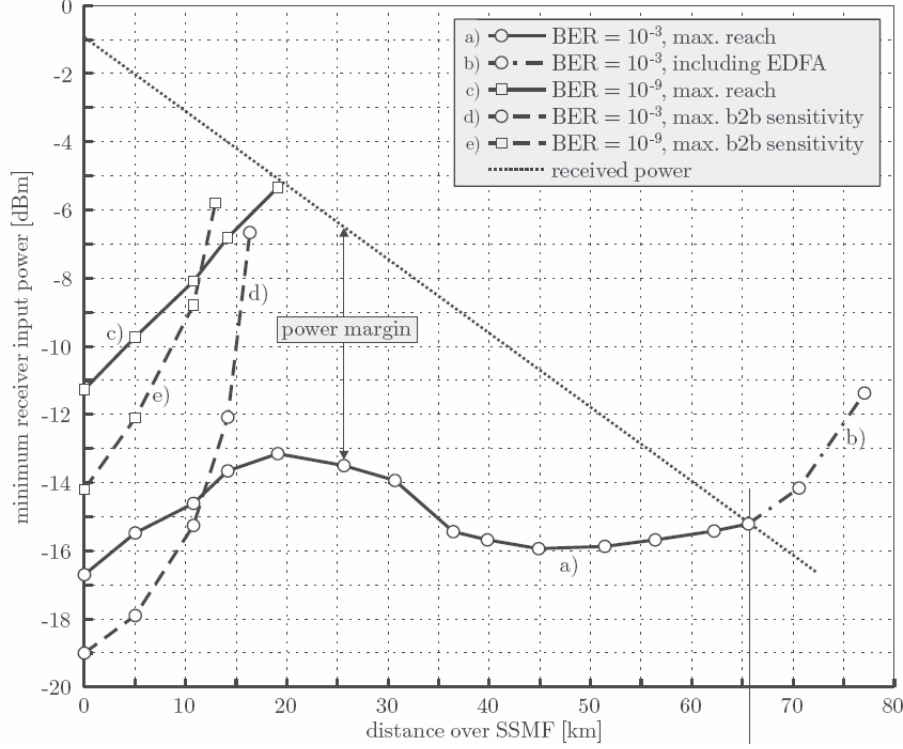


Figure 3.3: Minimum receiver input power versus transmission distance for the 1551 nm Vertilas VCSEL with PIN as receiver at a bit rate of 10.7 Gb/s [4].

The performance of the single-channel system at 10.7 Gb/s when using a DFB laser with EAM and an APD based receiver is shown in Figure 3.4. The dependence from the PRBS length is much smaller than in the case of the VCSEL in Figure 3.2. I achieved a maximum transmission distance of 57 km and 62 km for a PRBS length of $2^{31} - 1$ and $2^7 - 1$ respectively at a BER of 10^{-9} . This shows that the external modulated DFB laser has the same maximum transmission distance of 57 km at a PRBS length of $2^{31} - 1$ like the directly modulated VCSEL achieve with a PRBS length of $2^7 - 1$. The maximum transmission distances achieved at a BER of 10^{-3} equaled to 78 km and 89 km at a PRBS length of $2^{31} - 1$ and $2^7 - 1$ respectively. The 78 km at a PRBS length of $2^{31} - 1$ could not even be achieved with a PRBS length of $2^7 - 1$ with the VCSEL, which achieved only 71 km. Since the laser chirp is very small in comparison with a directly modulated laser and hence the impact of dispersion by the SSMF the s-shape of the curves above is not present in the case of an external modulated laser as can be seen from the figures.

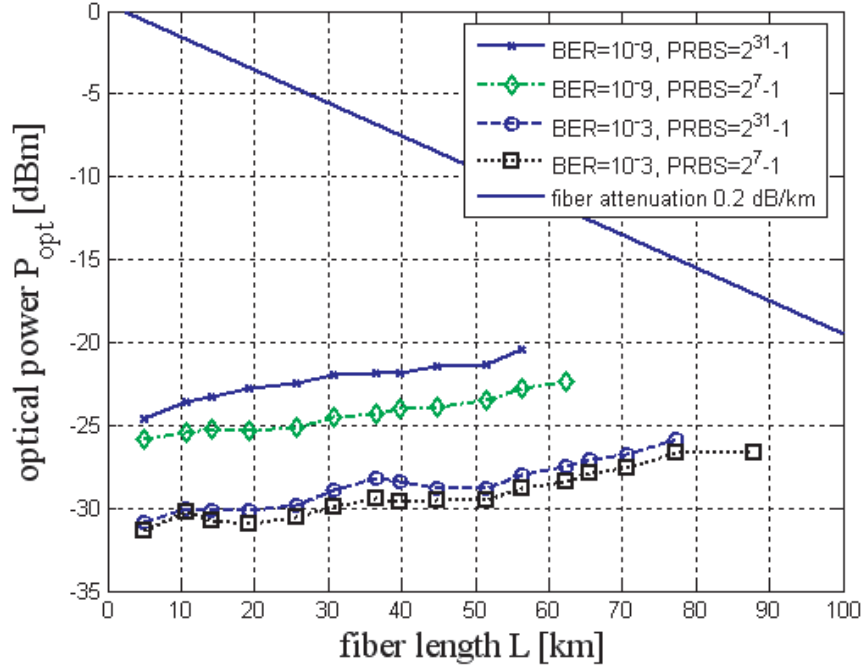


Figure 3.4: Minimum receiver input power versus transmission distance for the 1550 nm DFB laser with APD as receiver at a bit rate of 10.7 Gb/s.

Table 3.1 lists the driving conditions of the lasers optimized for maximum reach which were used in the measurements above. The DFB lasers driving conditions were the same for a BER of 10^{-9} as well as 10^{-3} , whereas they differ for the Vertilas 1551 nm VCSEL. Comparing these driving conditions with the optimum b2b driving conditions from section 2.2, it can be seen that a lower modulation voltage is chosen. This is done in order to reduce the laser chirp [27] and hence the influence of fiber induced dispersion on the pulses.

BER= 10^{-9}			
laser	APD Vertilas 1551 nm	PIN Vertilas 1551 nm	DFB 1550 nm
bias current	6 mA	-	60 mA
modulation voltage	260 mV _{pp}	-	530 mV _{pp}
BER= 10^{-3}			
laser	APD Vertilas 1551 nm	PIN Vertilas 1551 nm	DFB 1550 nm
bias current	6 mA	5.2 mA	60 mA
modulation voltage	500 mV _{pp}	1.22 V _{pp} (554 mV _{pp})	530 mV _{pp}

Table 3.1: Driving conditions for the lasers at a bit rate of 10.7 Gb/s (The voltage at the VCSEL (in braces) is lower than at the BERT due to a protection circuit between them).

3.1.3 Measurement results at 2.5 Gb/s

The measurements at 2.5 Gb/s and 1 Gb/s were only performed with an APD based receiver. The lasers in use were the Vertilas and RayCan VCSELs and the DFB laser with external modulation. Figure 3.5 shows a plot of the minimum required receive power, to achieve a certain BER, versus the fiber length for the Vertilas 1551nm VCSEL as the optical source at a bit rate of 2.5 Gb/s. At 2.5 Gb/s a less strong

pattern dependence is observed than at 10.7 Gb/s. The measured points do not differ significantly at short fiber lengths. The two upper curves are taken at a BER of 10^{-9} and show a transmission distance of 88 km with a PRBS length of $2^{31} - 1$ and 90 km at a PRBS length of $2^7 - 1$. While the two lower curves correspond to a BER of 10^{-3} . The achieved transmission distances at a PRBS length of $2^{31} - 1$ and $2^7 - 1$ correspond to a fiber length of 119 km and 129 km respectively.

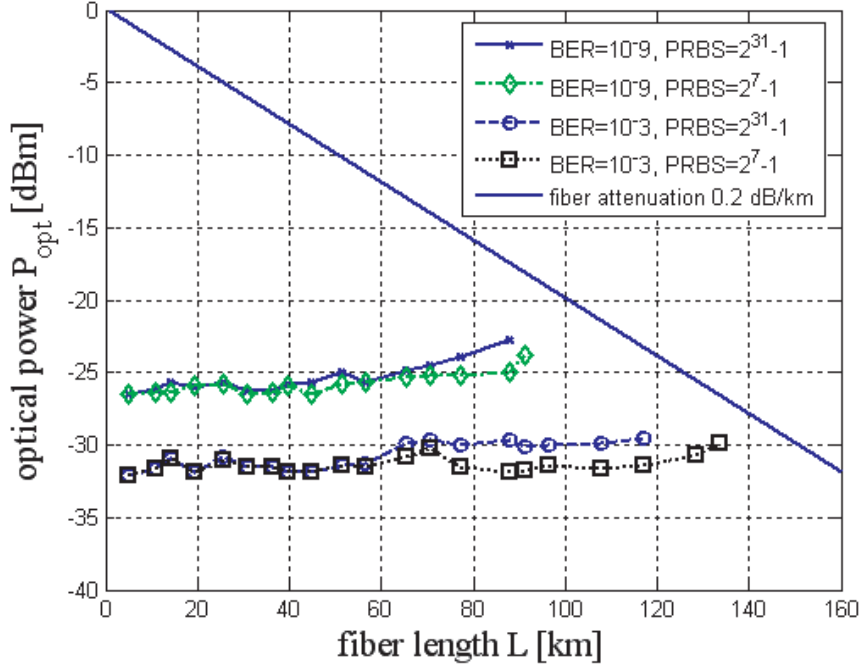


Figure 3.5: Minimum receiver input power versus transmission distance for the 1551 nm Vertilas VCSEL with APD as receiver at a bit rate of 2.5 Gb/s.

The results obtained with the 1538 nm RayCan VCSEL are shown in Figure 3.6. The curves at a BER of 10^{-9} show a maximum transmission distance of 95 km with a PRBS length of $2^{31} - 1$ and 98 km at a PRBS length of $2^7 - 1$. For a BER of 10^{-3} the achieved transmission distance at a PRBS length of $2^{31} - 1$ and $2^7 - 1$ correspond to 119 km and 129 km respectively, which is identical to the 1551 nm Vertilas laser. The results obtained with a DFB laser which serve as a reference are shown in Figure 3.7. The measurements show no pattern dependence. The curves at a BER of 10^{-9} show a transmission distance of 119 km. At a BER of 10^{-3} the achieved transmission distance corresponds to a fiber length of 148 km.

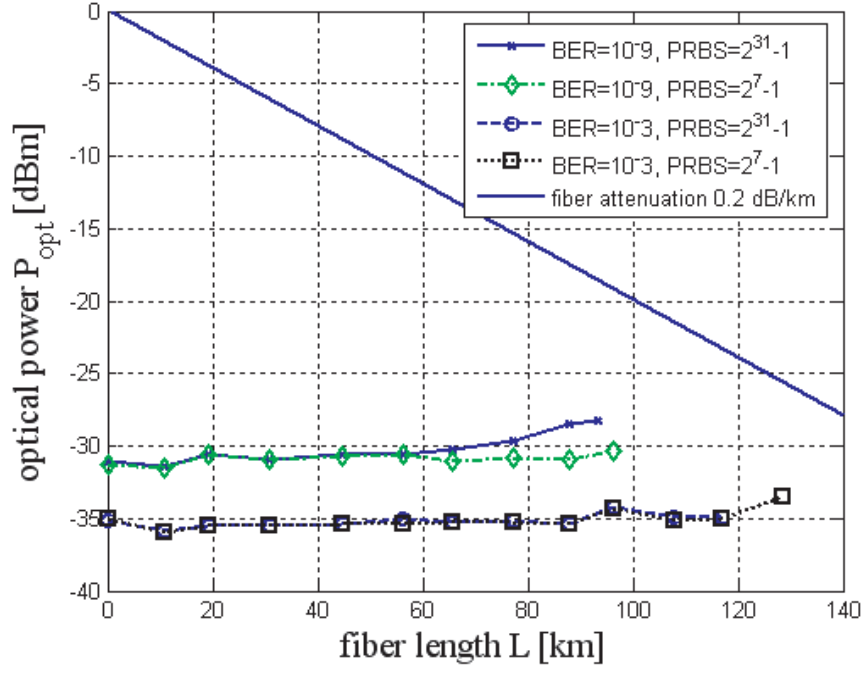


Figure 3.6: Minimum receiver input power versus transmission distance for the 1538 nm RayCan VCSEL with APD as receiver at a bit rate of 2.5 Gb/s.

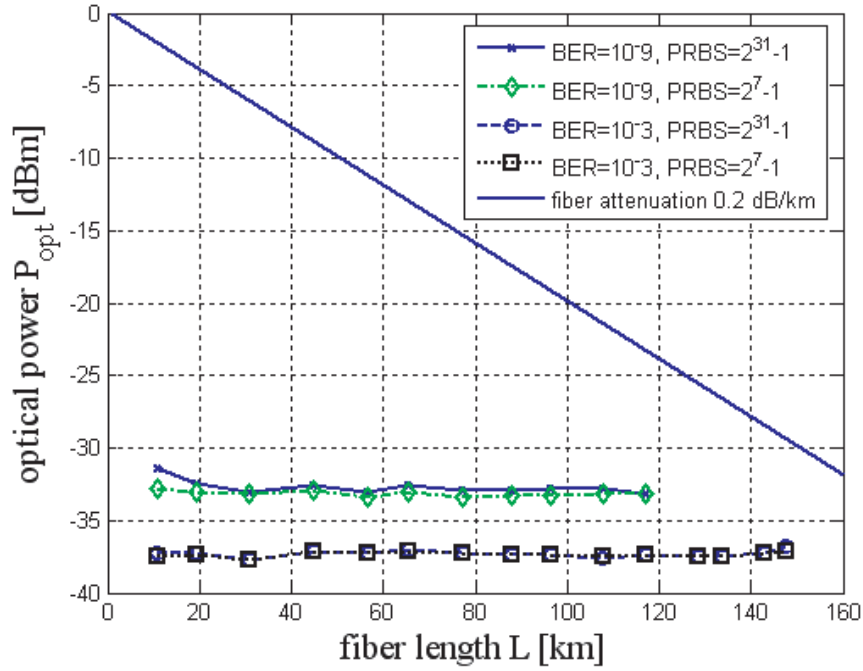


Figure 3.7: Minimum receiver input power versus transmission distance for the 1550 nm DFB laser with APD as receiver at a bit rate of 2.5 Gb/s.

Table 3.2 lists the driving conditions of the lasers optimized for maximum reach which were used for the 2.5 Gb/s measurements. The optimum driving conditions of the lasers again depend on the BER. For a BER of 10^{-9} the modulation voltage of the VCSELs is chosen smaller, for optimum performance, than for a BER of 10^{-3} . For the DFB laser the driving conditions remained the same for both BER's. The bias current of the 1538 nm RayCan VCSEL is chosen higher and the modulation voltage lower than in the b2b case.

BER= 10^{-9}			
laser	Vertilas 1551 nm	RayCan 1538 nm	DFB 1550 nm
bias current	6 mA	5.9	60 mA
modulation voltage	200 mV_{pp}	485 mV_{pp}	460 mV_{pp}
BER= 10^{-3}			
laser	Vertilas 1551 nm	RayCan 1538 nm	DFB 1550 nm
bias current	6 mA	5.9 mA	60 mA
modulation voltage	500 mV_{pp}	515 V_{pp}	460 mV_{pp}

Table 3.2: Driving conditions for the lasers at a bit rate of 2.5 Gb/s.

3.1.4 Measurement results at 1 Gb/s

Figure 3.8 shows a plot of the minimum required receive power, to achieve a certain BER, versus the fiber length for the Vertilas 1551nm VCSEL as the source at a bit rate of 1 Gb/s. The two upper curves at a BER of 10^{-9} show a transmission distance of 109 km with a PRBS length of $2^{31} - 1$ and 115 km at a PRBS length of $2^7 - 1$. The two lower curves correspond to a BER of 10^{-3} where a transmission distance of 142 km with a PRBS length of $2^{31} - 1$ and 155 km at a PRBS length of $2^7 - 1$ were achieved. The results obtained with the 1538 nm RayCan laser are shown in Figure 3.9. The curves at a BER of 10^{-9} show a transmission distance of 108 km with a PRBS length of $2^{31} - 1$ and 115 km at a PRBS length of $2^7 - 1$. For a BER of 10^{-3} the achieved transmission distance at a PRBS length of $2^{31} - 1$ and $2^7 - 1$ correspond to fiber lengths of 133 km and 142 km respectively.

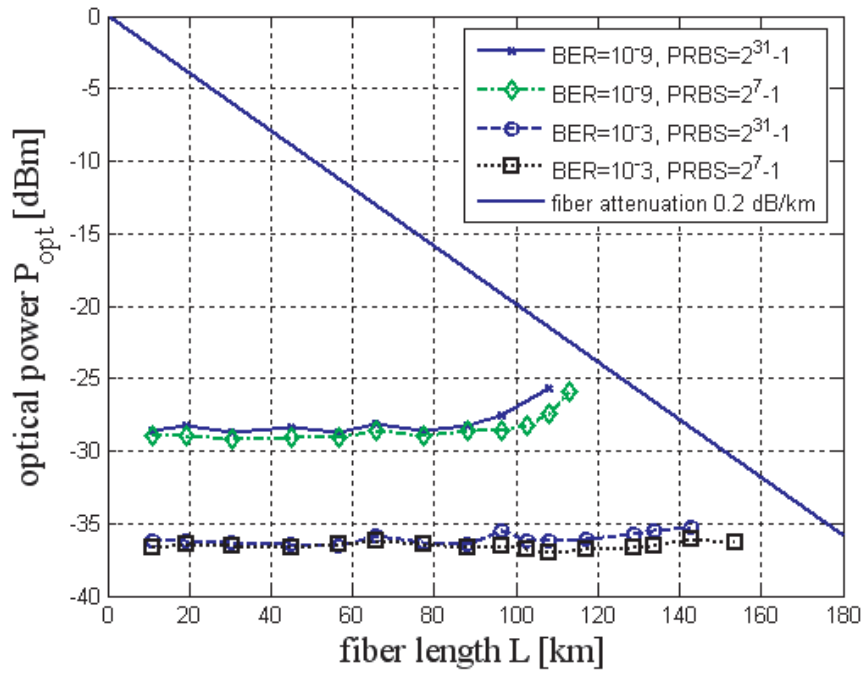


Figure 3.8: Minimum receiver input power versus transmission distance for the 1551 nm Vertilas VCSEL with APD as receiver at a bit rate of 1 Gb/s.

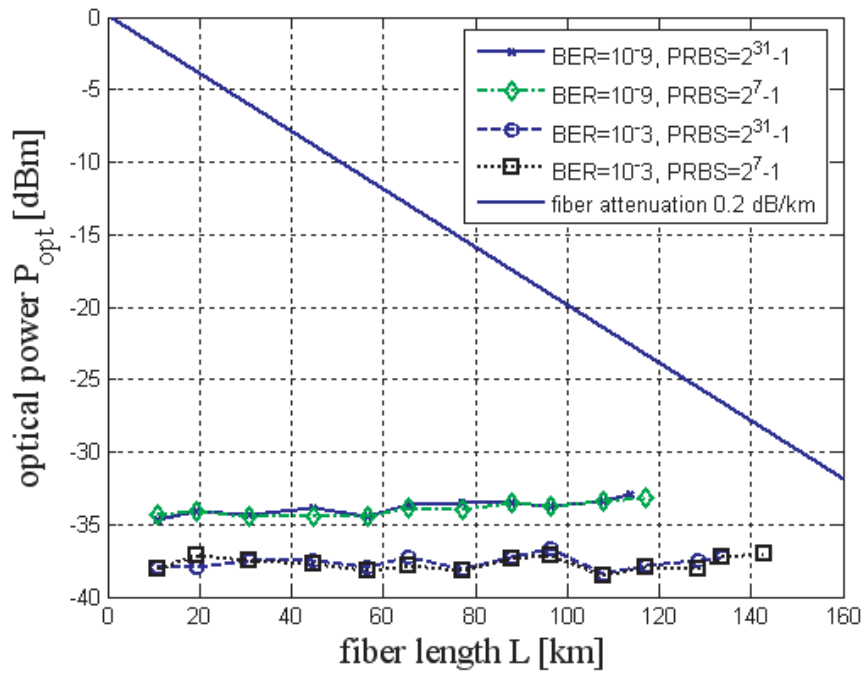


Figure 3.9: Minimum receiver input power versus transmission distance for the 1538 nm RayCan VCSEL with APD as receiver at a bit rate of 1 Gb/s.

The results obtained with the DFB laser are displayed in Figure 3.10. The measurements have not shown any pattern dependence with respect to the achieved fiber length, but differ in the sensitivity of the receiver. The curves at a BER of 10^{-9} show a transmission distance of 119 km regardless of the PRBS length. At a BER of 10^{-3} the achieved transmission distance equals to a fiber length of 148 km.

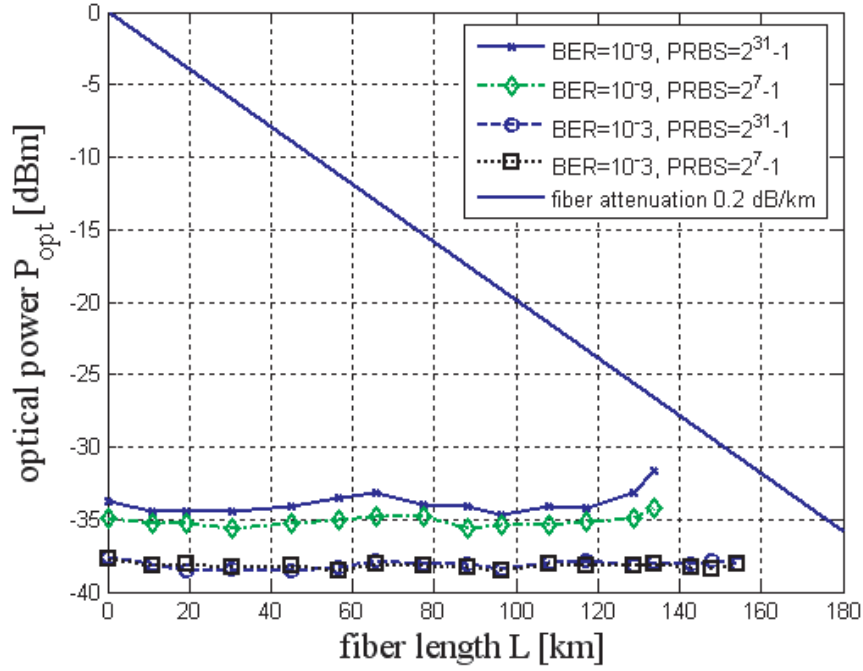


Figure 3.10: Minimum receiver input power versus transmission distance for the 1550 nm DFB laser with APD as receiver at a bit rate of 1 Gb/s.

Table 3.3 lists the driving conditions of the lasers optimized for maximum reach which were used for the 1 Gb/s measurements. For optimum performance at a BER of 10^{-9} the modulation voltage of the VCSELs is chosen smaller than for a BER of 10^{-3} . The DFB laser's driving conditions remained the same at both BER's. The bias current of the 1538 nm RayCan VCSEL is chosen higher and the modulation voltage lower than in the b2b case.

BER= 10^{-9}			
laser	Vertilas 1551 nm	RayCan 1538 nm	DFB 1550 nm
bias current	6 mA	5.9	60 mA
modulation voltage	270 mV_{pp}	480 mV_{pp}	530 mV_{pp}
BER= 10^{-3}			
laser	Vertilas 1551 nm	RayCan 1538 nm	DFB 1550 nm
bias current	6 mA	5.9 mA	60 mA
modulation voltage	690 mV_{pp}	590 V_{pp}	530 mV_{pp}

Table 3.3: Driving conditions for the lasers at a bit rate of 1 Gb/s.

3.2 4-channel CWDM system performance

The setup of the CWDM system which I have implemented is shown in Figure 3.11. The optical sources I use for the CWDM system are VCSELs from Vertilas and RayCan with a wavelength range from 1511 to 1591 nm. The four Vertilas VCSELs occupied four different CWDM bands from 1531 to 1591 nm. Three of the RayCan lasers are found to be within the 1531nm CWDM band with center wavelengths at 1524 nm, 1531 nm and 1538 nm. The fourth RayCan laser is within the 1511 nm band with a center wavelength of 1515 nm. The measurements are performed at bit rates of 10.7 Gb/s, 2.5 Gb/s and 1 Gb/s and a constant PRBS length of $2^{31} - 1$. For the receiver I use an APD diode (AT10XGC). The *data* output of the BERT N4906B is used to modulate the main transmission channel. The inverted output *data* is used to modulate an adjacent CWDM channel. Additionally the other two channels were modulated by the pattern generator HP70843A. Various lengths of electrical cables and fiber pigtails introduce a time delay and ensure a decorrelation of the data streams in all four channels on the common SSMF. The bias current for the VCSELs is provided via the bias tees from a current source (Thor Labs PRO800) which is not displayed in the schematic.

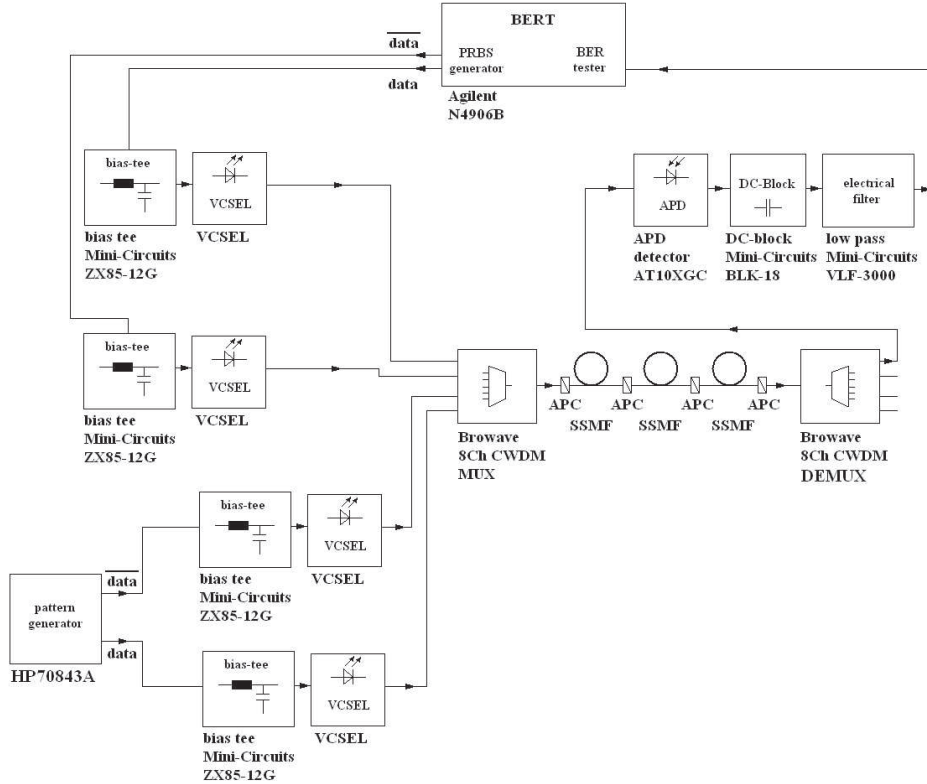


Figure 3.11: Setup for the 4-channel CWDM system performance measurement.

3.2.1 Measurement results at 10.7 Gb/s

Figure 3.12 depicts the sensitivity measurement results when using the APD diode with the Vertilas VCSELs at the maximum transmission distance and a bit rate of 10.7 Gb/s. The sensitivity measurements are performed at a BER of 10^{-3} in order to use enhanced FEC (since this results in a maximum final BER of 10^{-15}). Additionally, these measurements are also performed at a BER of 10^{-9} to show the degradation in maximum transmission distance compared to the case with BER 10^{-3} . All lasers driving conditions were optimized for maximum reach. The lines in the figure are power-curves and

illustrate the loss along the optical fiber of $\alpha_L = 0.2$ dB/km. The length of the arrows, which point to the measured receiver sensitivities at maximum reach, represent the insertion loss A_0 , which is caused by the multiplexer, the demultiplexer, splices, and the connectors. Figure 3.12(a) shows the achieved distances of 57 km for the 1531 and 1551 nm, and 51 km for the 1571 nm VCSEL at a BER of 10^{-3} . The 1591 nm VCSEL only achieved 35 km because of a reduced output power after being heated above 60°C in a previous measurement [4]. Comparing these results to a measurement performed with an PIN diode as receiver (depicted in Figure 3.13 [4]) a slight improvement by the use of the more sensitive APD diode can be achieved. With the PIN diode distances of 53 km at 1551 nm, 51 km at 1531 and 1571 nm, and 45 km at 1591 nm were measured. Figure 3.12(b) shows the results for a BER of 10^{-9} with the achieved distances of 28 km for the 1531 and 1551 nm, 25 km for the 1571 nm and 20 km for the 1591 nm VCSEL. Table 3.4 shows the driving conditions for the VCSELs. I found separate optimum driving conditions for a BER of 10^{-3} and for 10^{-9} . Due to the higher sensitivity of the APD diode the modulation voltage could be chosen lower than in the case of the PIN diode and therefore reducing the chirp involved. Which means a reduction of the impact of the dispersion of the SSMF. All lasers were therefore driven with a lower modulation voltage than in the b2b case for the purpose of minimization of the influence of the dispersion.

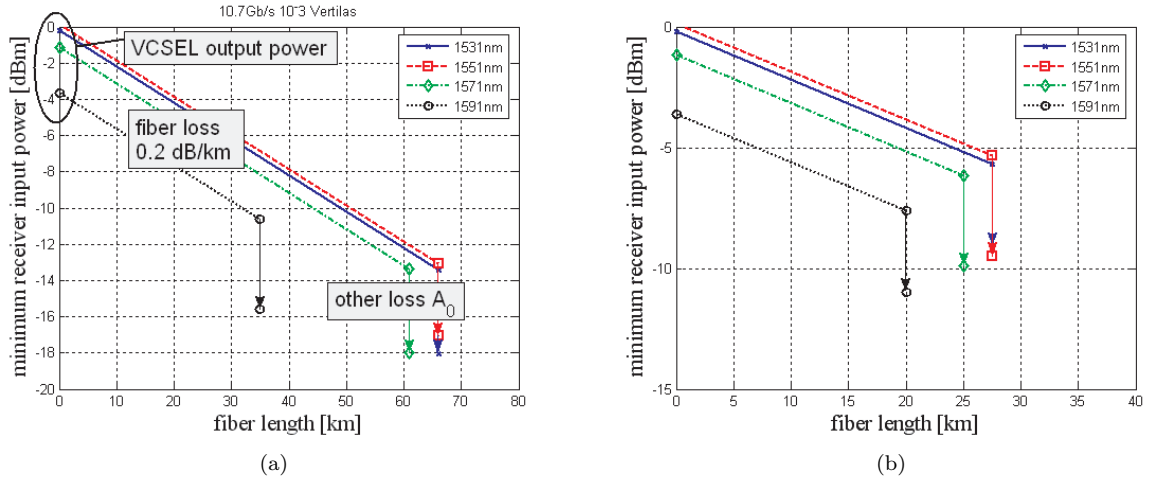


Figure 3.12: Sensitivity measurement result for the 1551 nm Vertilas VCSEL at a bit rate of 10.7 Gb/s with APD based receiver a) at 10^{-3} and b) at 10^{-9} .

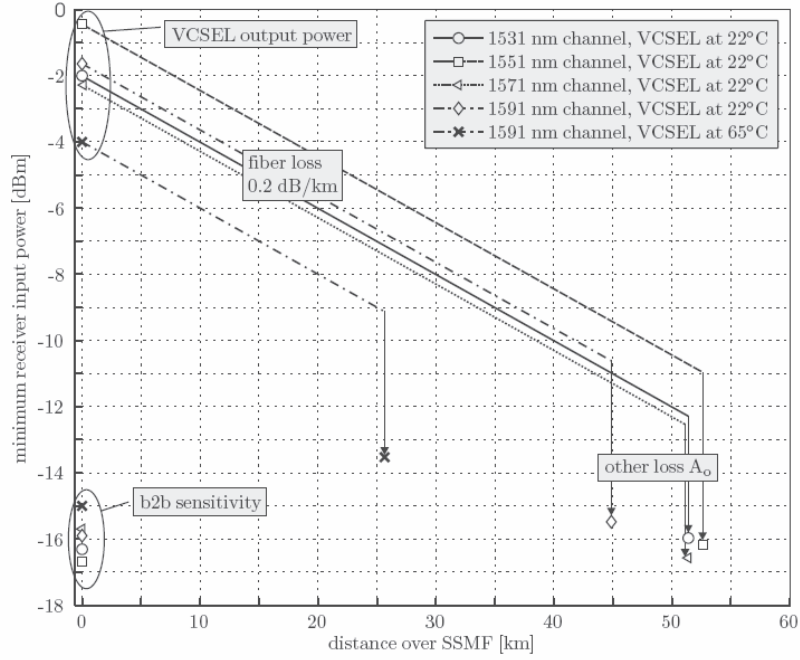


Figure 3.13: Sensitivity measurement result for the 1551 nm Vertilas VCSEL at a bit rate of 10.7 Gb/s with PIN diode as receiver[4].

APD receiver				
channel	1531 nm	1551 nm	1571 nm	1591nm
bias current modulation voltage	BER = 10^{-3}			
	6 mA 500 mV _{pp}	6 mA 500 mV _{pp}	6 mA 460 mV _{pp}	7.5 mA 520 mV _{pp}
bias current modulation voltage	BER = 10^{-9}			
	6 mA 500 mV _{pp}	6 mA 260 mV _{pp}	6 mA 460 mV _{pp}	7.5 mA 380 mV _{pp}
PIN receiver				
channel	1531 nm	1551 nm	1571 nm	1591nm
bias current modulation voltage	BER = 10^{-3}			
	4.4 mA 1.8 V _{pp} (610 mV _{pp})	6 mA 1.5 V _{pp} (556 mV _{pp})	6 mA 1.5 V _{pp} (560 mV _{pp})	7.5 mA 1.8 V _{pp} (605 mV _{pp})

Table 3.4: Driving conditions for the VCSELs at a bit rate of 10.7 Gb/s (The voltage at the VCSEL (in braces) is lower than at the BERT due to a protection circuit between them).

3.2.2 Measurement results at 2.5 Gb/s

The following sensitivity measurements are performed with the Vertilas and RayCan VCSELs at a bit rate of 2.5 Gb/s and a PRBS length of $2^{31} - 1$. An APD (AT10XGC) is used as optical receiver. Figure 3.14(a) depicts the sensitivity measurement result of the Vertilas lasers at a BER of 10^{-3} . The maximum transmission distance of 121 km is achieved with the 1551 nm VCSEL while the distance with the 1531 nm and 1571 nm VCSELs equaled 118 km. The shortest transmission distance of 101 km is achieved with the 1591 nm VCSEL. Figure 3.14(b) shows the results for a BER of 10^{-9} with achieved

transmission distances of 77 km with the 1551 nm VCSEL, 75 km at 1531 nm and 1571 nm. The achieved distance with the 1591 nm VCSEL equaled to 60 km.

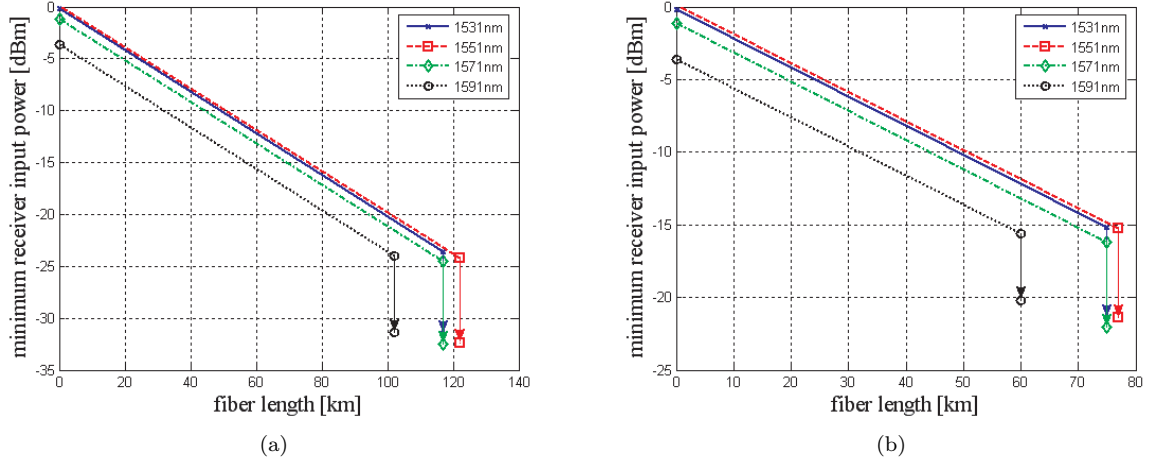


Figure 3.14: Sensitivity measurement result for the 1551 nm Vertilas VCSEL at a bit rate of 2.5 Gb/s with APD based receiver a) at 10^{-3} and b) at 10^{-9} .

The RayCan lasers have a slightly lower output power of about -3 dBm but a cleaner modulation and hence better eye diagrams than the Vertilas lasers. Therefore similar distances as with the Vertilas VCSELs were achieved with the RayCan VCSELs depicted in Figure 3.15(a) at a BER of 10^{-3} . The transmission distance of all lasers equaled 112 km. At a BER of 10^{-9} (depicted in Figure 3.15(b)) the transmission distance of the 1531 nm and the 1538 nm VCSELs equaled 87 km, and 81 km for the other two VCSELs. With the other two VCSELs (at 1515 nm and 1524 nm) 81 km could be achieved.

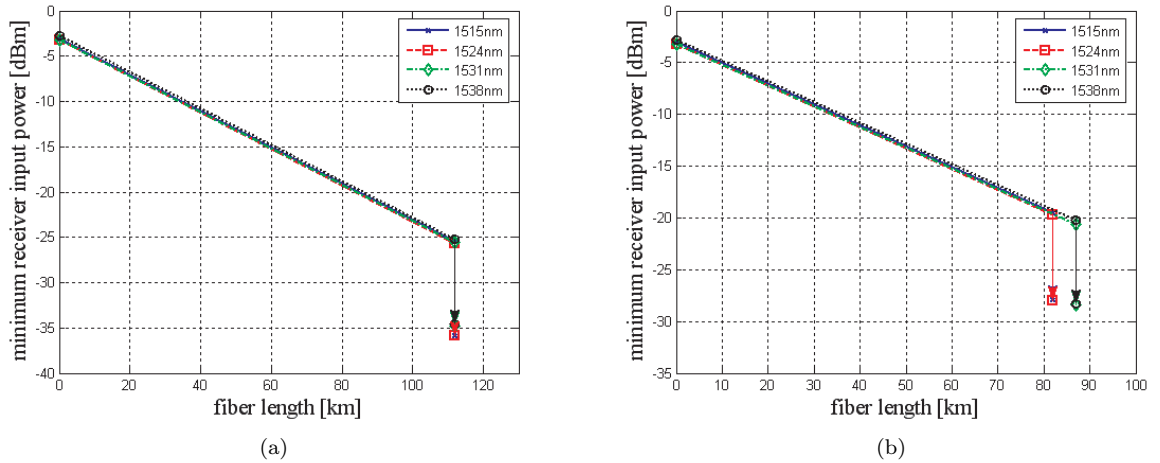


Figure 3.15: Sensitivity measurement result for the 1538 nm RayCan VCSEL at a bit rate of 2.5 Gb/s with APD based receiver a) at 10^{-3} and b) at 10^{-9} .

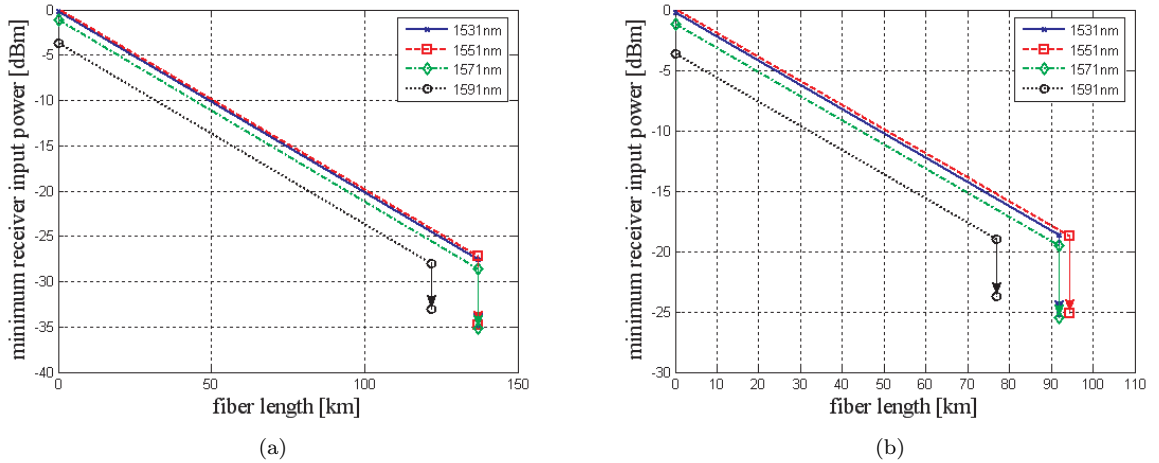
The driving conditions for the VCSELs are listed in Table 3.5, again with different values for a BER of 10^{-3} and 10^{-9} . The bias current is chosen higher than in the b2b case, and the modulation voltage is lower in order to reduce the laser chirp. The modulation voltage that is chosen to achieve a BER of 10^{-9} is smaller than for a BER of 10^{-3} .

APD receiver with Vertilas lasers				
channel	1531 nm	1551 nm	1571 nm	1591nm
bias current modulation voltage	BER = 10^{-3}			
	6 mA 580 mV _{pp}	6 mA 500 mV _{pp}	6 mA 520 mV _{pp}	7.5 mA 530 mV _{pp}
bias current modulation voltage	BER = 10^{-9}			
	6 mA 300 mV _{pp}	6 mA 200 mV _{pp}	6 mA 340 mV _{pp}	7.5 mA 240 mV _{pp}
APD receiver with RayCan lasers				
channel	1511 nm	1524 nm	1531 nm	1538nm
bias current modulation voltage	BER = 10^{-3}			
	6 mA 580 mV _{pp}	6.1 mA 520 mV _{pp}	6 mA 585 mV _{pp}	5.9 mA 515 mV _{pp}
bias current modulation voltage	BER = 10^{-9}			
	6 mA 500 mV _{pp}	6.1 mA 450 mV _{pp}	6 mA 410 mV _{pp}	5.9 mA 485 mV _{pp}

Table 3.5: Driving conditions for the VCSELs at a bit rate of 2.5 Gb/s.

3.2.3 Measurement results at 1 Gb/s

The following sensitivity measurements are performed with the Vertilas and RayCan VCSELs at a bit rate of 1 Gb/s and a PRBS length of $2^{31} - 1$. Again an APD (AT10XGC) is used as optical receiver. Figure 3.16(a) depicts the sensitivity measurement result of the Vertilas lasers at a BER of 10^{-3} . A transmission distance of 125 km is achieved with the 1591 nm VCSEL, with the three other lasers a maximum transmission distance of 140 km is achieved. Figure 3.16(b) shows the results for a BER of 10^{-9} with achieved transmission distances of 94.5 km with the 1551 nm VCSEL, 92 km with the 1531 nm VCSEL and the 1571 nm VCSEL. The achieved distance with the 1591 nm VCSEL equaled 77 km.

Figure 3.16: Sensitivity measurement result for the 1551 nm Vertilas VCSEL at a bit rate of 1 Gb/s with APD based receiver a) at 10^{-3} and b) at 10^{-9} .

Similar distances as with the Vertilas VCSELs were achieved with the RayCan VCSELs as depicted in Figure 3.15(a) at a BER of 10^{-3} . The maximum transmission distance of 119.5 km is achieved with the 1531 nm VCSEL and the 1538 nm VCSEL, while the distance at 1515 nm and 1524 nm equaled

117 km. At a bit rate of 10^{-9} (depicted in Figure 3.15(b)) the transmission distance of the 1531 nm VCSEL and the 1538 nm VCSEL equaled 102 km, and 97 km for the other two VCSELs at 1515 nm and 1524 nm.

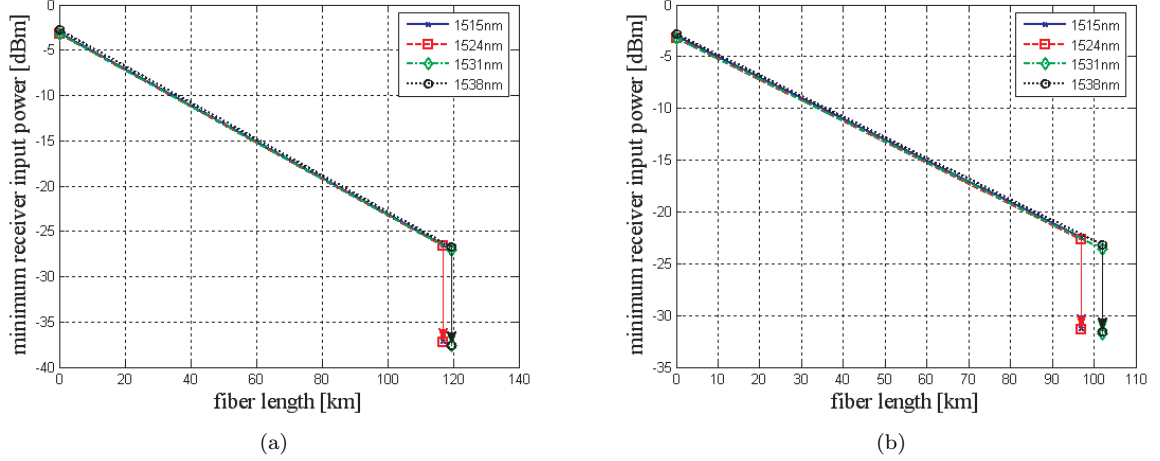


Figure 3.17: Sensitivity measurement result for the 1538 nm RayCan VCSEL at a bit rate of 1 Gb/s with APD based receiver a) at 10^{-3} and b) at 10^{-9} .

The driving conditions for the VCSELs are listed in Table 3.6, again with different values for a BER of 10^{-3} and 10^{-9} . Also at a bit rate of 1 Gb/s the bias current is chosen higher than in the b2b case, and the modulation voltage is lower to reduce the laser chirp. The modulation voltage that is chosen to achieve a BER of 10^{-9} is smaller than at a BER of 10^{-3} .

APD receiver with Vertilas lasers				
channel	1531 nm	1551 nm	1571 nm	1591 nm
bias current modulation voltage	BER = 10^{-3}			
	6 mA 350 mV _{pp}	6 mA 270 mV _{pp}	6 mA 370 mV _{pp}	7.5 mA 320 mV _{pp}
bias current modulation voltage	BER = 10^{-9}			
	6 mA 700 mV _{pp}	6 mA 690 mV _{pp}	6 mA 710 mV _{pp}	7.5 mA 680 mV _{pp}
APD receiver with RayCan lasers				
channel	1511 nm	1524 nm	1531 nm	1538 nm
bias current modulation voltage	BER = 10^{-3}			
	6 mA 600 mV _{pp}	6.1 mA 580 mV _{pp}	6 mA 600 mV _{pp}	5.9 mA 590 mV _{pp}
bias current modulation voltage	BER = 10^{-9}			
	6 mA 520 mV _{pp}	6.1 mA 470 mV _{pp}	6 mA 400 mV _{pp}	5.9 mA 480 mV _{pp}

Table 3.6: Driving conditions for the VCSELs at a bit rate of 1 Gb/s.

3.3 HD-video transmission via CWDM system

To test the performance of the CWDM system within a real data transmission environment I transmitted a digital video signal and measured the achievable maximum transmission distance. Both, a single channel measurement and a multichannel measurement were performed. The transmitted signal is a high definition serial digital interface (HD-SDI) signal which is standardized by the society of motion picture and television engineers (SMPTE) [28]. The HD-SDI standard provides a nominal data rate of 1.485 Gb/s and is intended for use in the transmission of uncompressed, unencrypted digital video signals (optionally including embedded audio) within television facilities. Beside this standard there is also serial digital interface (SDI) [29] at a bit rate of 270 Mb/s and 3 gigabit-SDI (3G-SDI) [30] at a bit rate of 2.97 Gb/s. In contrast to 3G-SDI which uses only one coaxial cable there also exists Dual Link HD-SDI [31] which uses two coaxial cables to achieve a total bit rate of 2.97 Gb/s. The various serial digital interface standards all use one or more coaxial cables with BNC connectors with a nominal impedance of $75\ \Omega$. The maximum transmission distance without repeaters over coaxial cables is 300 m for SDI and 100 m for HD-SDI. The specified signal amplitude at the source is 800 mV ($\pm 10\%$) peak-to-peak. Data is encoded in non return to zero (NRZI) format, and a linear feedback shift register is used to scramble the data to reduce the likelihood that long strings of zeroes or ones will be present on the interface. The interface synchronizes itself by means of a clock recovery. The start of a frame is detected by a special synchronization pattern, which consists of a sequence of ten ones followed by twenty zeroes in SDI and twenty ones followed by forty zeroes in HD-SDI. This bit pattern can not be used anywhere else within the data payload. A single channel measurement and a multichannel measurement are performed to determine the maximum distance over which a transmission is possible.



Figure 3.18: Backside of the DVI HD-SDI signal converters.

Figure 3.19 shows the setup of the single channel system for the HD-SDI digital video signal transmission. As signal source I use a PC with two video outputs, a digital visual interface (DVI) and a video graphics array (VGA) output. Monitor 1 is connected to the VGA output. The digital signal of the DVI output is converted to a serial digital HD-SDI signal by a converter (shown in Figure 3.18, lower device). To achieve an optimum performance with the VCSEL a variable electrical attenuator is used to adjust the modulation swing of the HD-SDI signal which is supplied to the VCSEL via a bias-tee. The bias current is supplied by a current source from Thor Labs (PRO800) which is also used for biasing the other VCSELs. The optical signal is transmitted over a SSMF which introduces dispersion to the signal. The signal is received with the APD and converted into the electrical domain. The maximum peak-to-peak output voltage of the APD is 165 mV, but the HD-SDI to DVI converter requires a voltage of 400 mV peak-to-peak. Therefore I use an amplifier with a constant amplification of 20 dB and an attenuator to adjust the signal for best performance. Since the HD-SDI converter already has a built in filter I omit using an electrical filter after the APD because it lead to a shorter maximum fiber distance.

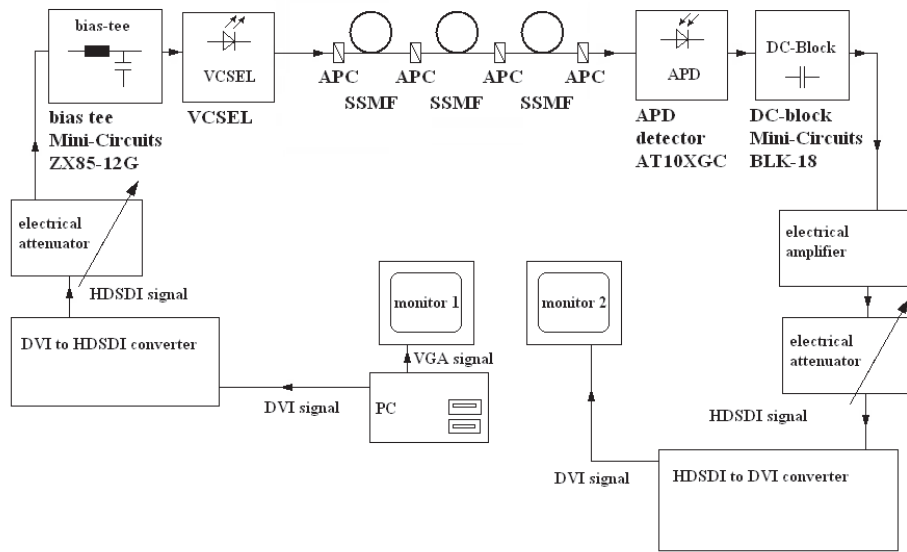


Figure 3.19: Measurement setup for the single channel transmission of the HD-SDI signal.

The setup for the multi channel measurement is shown in Figure 3.20 and has an additional multiplexer and demultiplexer. The optical signals are multiplexed into a SSMF and at the receiving end there is a DEMUX to separate the wavelengths and direct the HD-SDI signal into the APD receiver. Two neighboring lasers are modulated by the pattern generator of the BERT to emulate other active channels. Figure 3.21 shows a photo of the laboratory setup with the two monitors, the converters, and the SSMF. Figure 3.22 shows the components used in more detail.

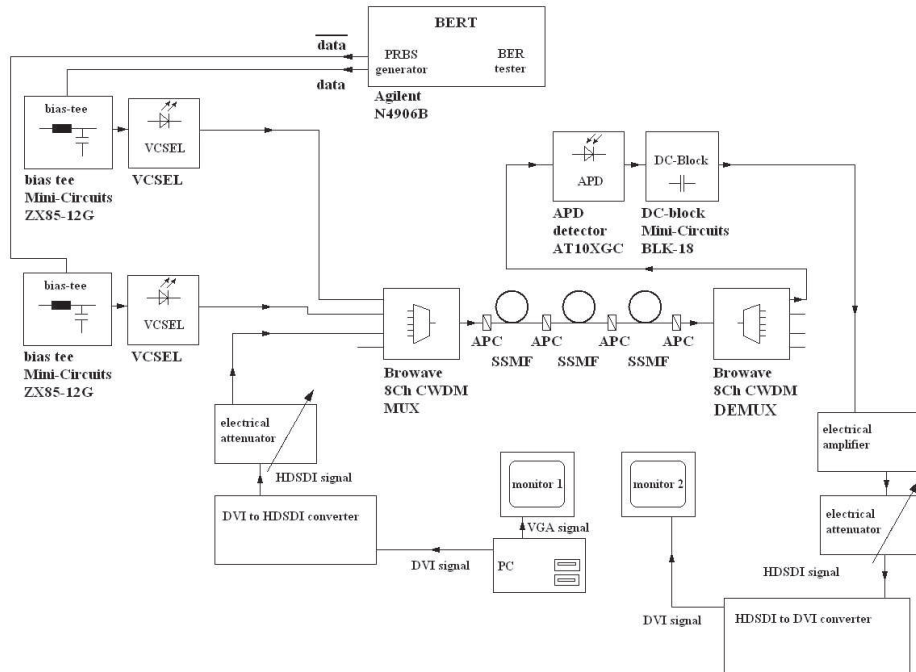


Figure 3.20: Measurement setup for the multi channel transmission of the HD-SDI signal.

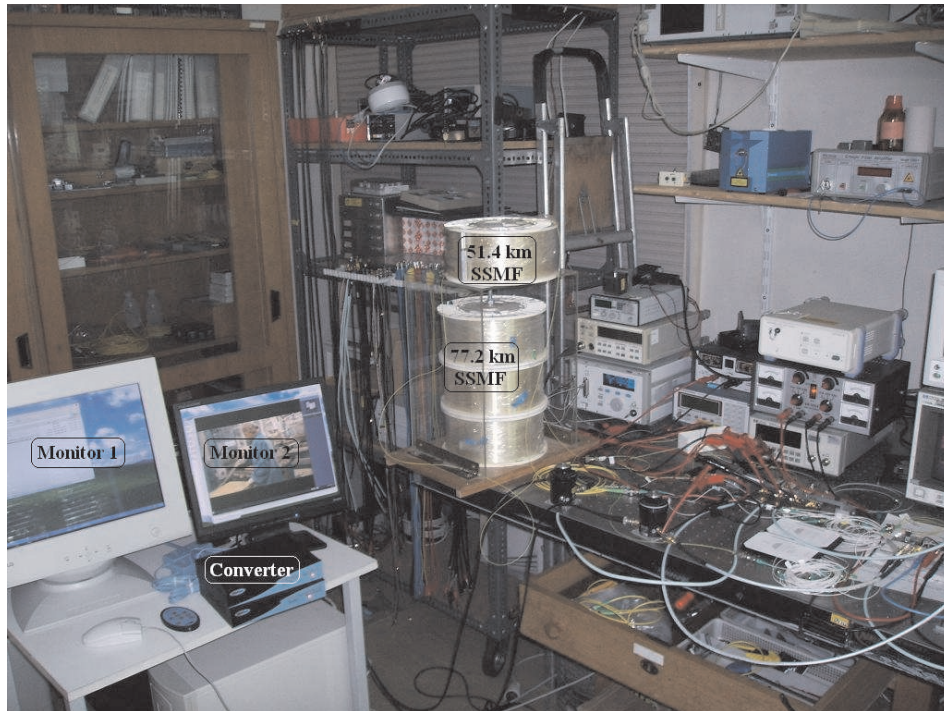


Figure 3.21: Laboratory setup with two monitors, the spools of SSMF, and the signal converters.

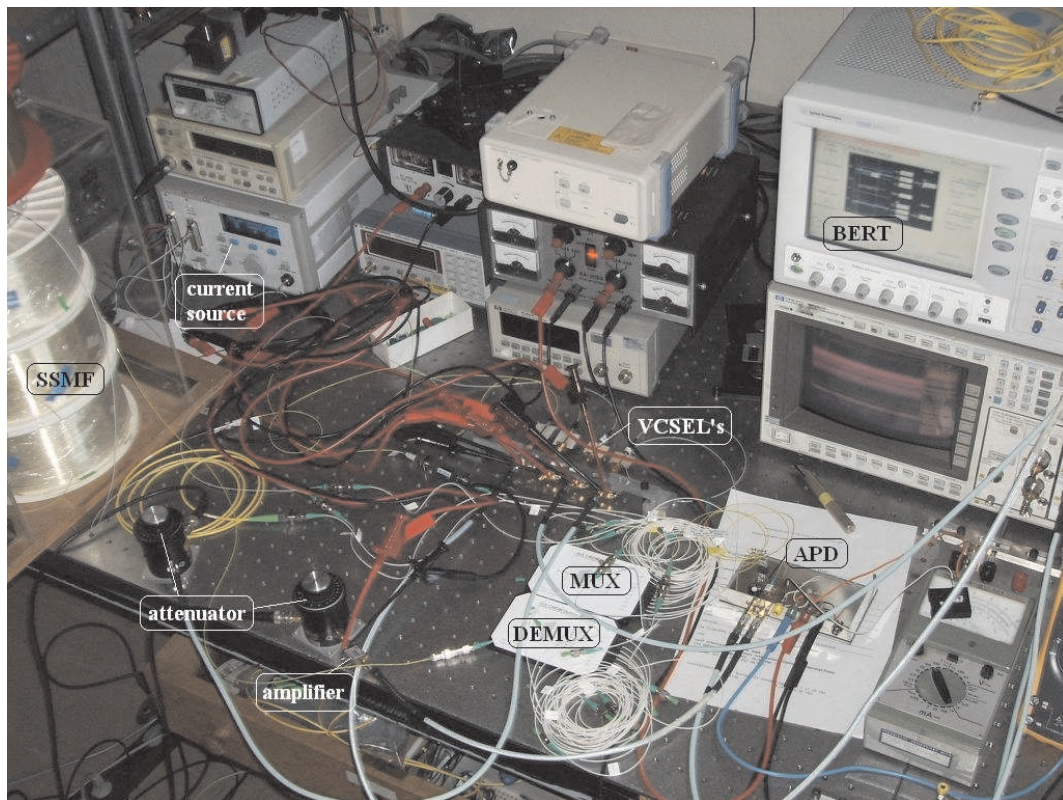


Figure 3.22: Photo of the components which are used for the transmission of the HD-SDI signal.

Table 3.7 shows the achieved transmission distances over the SSMF for all lasers in the case of single channel and multi channel transmission. The 1591 nm Verilas laser has a significantly shorter maximum transmission distance because its output power decreased permanently after being heated up over 50 °C in a previous measurement. A very large transmission distance of over 100 km is achieved for all lasers. This is much more than the distances achieved for BER 10^{-9} , PRBS of $2^{31} - 1$ and bit rate of 1 Gb/s in section 3.1 and 3.2. That is explained by the fact that in the HD-SDI standard a linear feedback shift register is used to scramble the data in order to reduce the likelihood of long strings of ones or zeros. The transmission distance could be significantly increased through the use of an additional FEC unit which can reduce a BER of 10^{-3} below 10^{-9} . Comparing this with the results in section 3.1 and 3.2 a transmission over a distance of 150 km and more is possible.

Laser	single channel without multiplexer's	multi channel
RayCan 1515 nm	107 km	102 km
RayCan 1524 nm	107 km	102 km
RayCan 1531 nm	107 km	102 km
RayCan 1538 nm	107 km	102 km
Vertilas 1531 nm	107 km	102 km
Vertilas 1551 nm	107 km	102 km
Vertilas 1571 nm	107 km	102 km
Vertilas 1591 nm	83.5	87 km

Table 3.7: Achieved transmission distances with the different lasers.

3.4 Conclusion

An unidirectional 4-channel CWDM transmission over standard single-mode fiber was experimentally demonstrated. The transmission system was based on commercially available, non preselected, uncooled long wavelength VCSELs, which were directly modulated at a bit rate of 10.7 Gb/s, 2.5 Gb/s and 1 Gb/s. A pattern dependence was observed which suggests the use of a coding that prevents long strings of ones or zeros, whose beneficial effect could be seen in the transmission of a HD-DVI signal. The performance enhancement when using an APD diode instead of an PIN diode was evaluated. It showed a significant increase in the transmission distance and allowed to achieve the dispersion limited reach. The use of an SOA for further performance improvement showed that the high ASE generated by the SOA prevents a beneficial use in the system. The transmission of a HD-DVI signal at 1.485 Gb/s over a distance of more than 100 km has shown the proper functionality in the field.

In future research projects related to this work, it would be interesting to address the following topics:

1. A performance demonstration of a forward error correction unit together with the use of electronic dispersion compensation (EDC) might enhance sensitivity and reachable distance, especially in the case of high dispersion.
2. An examination of SOA's from other vendors with lower ASE noise generation, which could be more beneficial in the regeneration of the signal.
3. A detailed cost-performance analysis for optical access networks like fiber-to-the-home (FTTH).

Appendices

Appendix A

Datasheets

A1. APD diode (AT10XGC)

Operating Characteristics

Case Temperature = 25°C unless otherwise specified

Parameter	Symbol	Measurement Conditions	Min	Typ	Max	Unit
Optical sensitivity BOL [1] [2]	Sens	2 ³¹ -1 PRBS BER<10 ⁻¹² V _{APD} =V _{M10}		-26.5	-25.0	dBm
Sensitivity penalty EOL over temperature [1] [2]		2 ³¹ -1 PRBS BER<10 ⁻¹² V _{APD} =V _{M10} T=-5 to +75°C		0.75	1.0	dB
Deviation from linear phase		DC - 6GHz	-10		+10	°
High frequency -3dB corner	f _H	V _{APD} =V _{M10} Small signal	7	7.5		GHz
Low frequency -3dB corner	f _L				40	kHz
Transimpedance gain [2] [4] [5]	T _Z	Small signal	1.1	1.6	2.3	kΩ
Maximum output voltage ⁶	V _{OUT}	Peak-to-peak		600	700	mV
Return loss	S ₂₂	DC to 7.0GHz			-8	dB
Optical overload [2]	P _{SAT}	0dB Attenuation V _{APD} =V _{M3} BER<10 ⁻¹²	-3	-1		dBm
Optical overload extension		With VOA actuated	+13			dBm
APD breakdown voltage	V _{br}	T=25°C I _{APD} =10mA	25		40	V
APD breakdown voltage temperature coefficient	T _{Vbr}		0.030	0.045	0.061	V/°C
Dark current	I _d	At 90% of V _{br}			100	nA
Amplifier bias current	I _{OC}			75	95	mA
Input current for output limiting	I _{in lim}	Peak-to-peak		0.5		mA
VOA maximum attenuation	Att		20	30		dB
VOA control voltage [7]	V _{Att}	Attenuation = 20dB		5.5	9	V
VOA current	I _{Att}	Attenuation = 20dB		6	7.2	mA
VOA power dissipation (continuous)	P _{Att}	Attenuation = 20dB		33	65	mW
VOA response time [8]		From attenuation = 1dB to 20dB		5	10	ms
Polarisation dependent loss	PDL	VOA unbiased			0.15	dB
Polarisation dependent loss	PDL	VOA biased			0.4	dB
Thermistor resistance	R _{TH}	T=25°C		10		kΩ

A2. PIN diode (R2860C)

Absolute Maximum Ratings

Parameter	Symbol	Min	Max	Unit
Operating Temperature Range	TOP	−5	70	°C
Storage Case Temperature Range	Tstg	−40	85	°C
Preamplifier Supply Voltage	VCC	—	12	V
Photodiode Bias Voltage	VPD	—	20	V
Optical Input Power	PIN	—	4	dBm

Electrical/Optical Characteristics

Table 1. Electrical and Optical Characteristics (25 °C Case Temperature)

Parameter	Symbol	Min	Typ	Max	Unit
Optical Wavelength Range	λ	1280	—	1580	nm
Sensitivity (10^{-10} BER, PRBS $2^{23} - 1$)	—	—	−20	−18	dBm
Overload (10^{-13} BER, PRBS $2^{23} - 1$)	—	0	2	—	dBm
Responsivity	R	0.7	0.8	—	A/W
Dark Current	Id	—	—	1	nA
High-Frequency Cutoff	—	8.0	9.0	—	GHz
Low-Frequency Cutoff	—	—	—	30	kHz
Transimpedance	Z	1400	2000	—	Ω
Maximum ac Output Voltage Swing	—	—	800	—	mVp-p
RF Output Return Loss* (0.1 GHz—5 GHz)	RLRF	—	—	10	dB
Optical Return Loss	ORL	27	—	—	dB
Logic Sense	—	—	Noninverting	—	—
Preamplifier Supply Voltage	(VCC)	7.6	8.0	8.4	V
Photodiode Supply Voltage	VPD	7	8	12	V
Supply Current	Icc	—	80	120	mA

A3. SOA (BOA1004)

Parameter		Min	Typ	Max	
Operating Current	I_{OP}		500	600	mA
Central Wavelength	λ_C	1530	1550	1570	nm
ASE Optical 3 dB Bandwidth	BW	80	85		nm
Saturation Output Power @ -3 dB	P_{SAT}	13	15		dBm
Small Signal Gain across BW @ Pin = -20 dBm	G	20	24		dB
Gain Ripple (p-p) @ I_{OP}	δG		0.05	0.2	dB
Polarization Extinction Ratio	PER		18		dB
Noise Figure	NF		7.5	9	dB
Forward Voltage	V_F		1.3	1.6	V
TEC Operation (typ / max @ $T_{CASE} = 25^\circ\text{C} / 70^\circ\text{C}$)					
- TEC Current	I_{TEC}		0.13	1.5	A
- TEC Voltage	V_{TEC}		0.28	3.5	V
- Thermistor Resistance	R_{TH}		10K		Ω
SPECIFICATIONS ARE SUBJECT TO CHANGE WITHOUT NOTICE					

Abbreviations

List of abbreviations

3G-SDI	3 gigabit serial digital interface
ADSL	asynchronous digital subscriber line
APC	angled polished connector
APD	avalanche photodiode
ASE	amplified spontaneous emission
B2B	back to back
BER	bit error ratio
CWDM	coarse wavelength division multiplexing
DEMUX	demultiplexer
DFB	distributed feedback laser
DVI	digital visual interface
DWDM	dense wavelength division multiplexing
EAM	electro-absorption modulator
EDFA	Erbium doped fiber amplifier
FEC	forward error correction
FTTB	fiber to the building
FTTC	fiber to the curb
FTTH	fiber to the home
HD-SDI	high definition serial digital interface
IC	integrated circuit
ITU	International Telecommunications Union
ISDN	integrated services digital network
MUX	multiplexer
NRZI	non-return-to-zero-inverted
NTC	negative temperature coefficient
PCB	printed circuit board
PIN	positive intrinsic negative
PON	passive optical network
PRBS	pseudo random bit sequence
RB	resolution bandwidth
SDI	serial digital interface
SMD	surface mounted device
SMPTE	society of motion picture and television engineers
SOA	semiconductor optical amplifier
SONET	synchronous optical network
SSMF	standard single mode fiber
SSMR	side mode suppression ratio
TFF	thin film filter
VCSEL	vertical cavity surface emitting laser
WDM	wavelength division multiplexing

Bibliography

- [1] K. G. Coffman and A. M. Odlyzko, "Growth of the internet," *Optical Fiber Telecommunications IV B*, Academic Press, I. Kaminow and T. Li (ed.), pp. 17–57, 2002.
- [2] ITU-T, *G.694.2, Spectral grids for WDM applications: CWDM wavelength grid*, International Telecommunication Union, 2002.
- [3] ITU-T, *G.694.1, Spectral grids for WDM applications: DWDM frequency grid*, International Telecommunication Union, 2002.
- [4] C. Hambeck, "Performance enhancement in multi-wavelength systems using vertical-cavity surface-emitting lasers," Diploma Thesis, Institute of Communications and Radio-Frequency Engineering, Vienna University of Technology, 2006.
- [5] F. Fidler, "Performance enhancement in WDM-systems," Diploma Thesis, Institute of Communications and Radio-Frequency Engineering, Vienna University of Technology, 2004.
- [6] S. Cerimovic, "Vertical-cavity surface-emitting laser als Quellen in optischen Übertragungssystemen bei einer Wellenlänge von 1550 nm," Diploma Thesis, Institute of Communications and Radio-Frequency Engineering, Vienna University of Technology, 2005.
- [7] ITU-T, *G.709, Interfaces for the Optical Transport Network (OTN)*, International Telecommunication Union, 2003.
- [8] ITU-T, *G.975, Forward error correction for submarine systems*, International Telecommunication Union, 2000.
- [9] Applied Micro Circuits Corporation (AMCC), DispersionXX-2 chipset. (2006). [Online]. Available: www.amcc.com
- [10] RayCan. [Online]. Available: www.raycan.com
- [11] Vertilas. [Online]. Available: www.vertilas.com
- [12] S. Riyopoulos, *Elimination of cavity relaxation oscillations using photoactive pumping*, Science Applications International Corporation, 1999.
- [13] W. Leeb, *Optische Nachrichtentechnik ONT, Skriptum VO 389.077*, Institut für Nachrichtentechnik und Hochfrequenztechnik, Technische Universität Wien, 2005.
- [14] Bookham Inc., High sensitivity 10Gb/s surface mount coplanar APD preamp receiver AT10XGC. (2006). [Online]. Available: www.bookham.com
- [15] National Semiconductor Corporation, +3.3V voltage stabilizer LM1117MP-3.3 datasheet. (2006). [Online]. Available: www.national.com
- [16] National Semiconductor Corporation, 1.25V-37V variable voltage stabilizer LM317 datasheet. (2007). [Online]. Available: www.national.com

- [17] STMicroelectronics GROUP OF COMPANIES, +5V voltage stabilizer L7805ACV datasheet. (2008). [Online]. Available: www.st.com
- [18] Ericsson Microelectronics, DFB with EAM PGT 204 04 datasheet. (2000). [Online]. Available: www.datasheetcatalog.com
- [19] S. Aleksic, *Techik der Kommunikationsnetze, Teil A: Hardware Komponenten, Systeme und Schnittstellen, Script VO 388.031*, Institute for Wideband Communication, Vienna University of Technology, 2006.
- [20] itwissen. [Online]. Available: www.itwissen.info/definition/lexikon/3R-Regeneration-3R-shaping-re-amplification-re-timing.html
- [21] COVEGA Corporation, Booster Optical Amplifier BOA1004 datasheet. (2007). [Online]. Available: www.covega.com
- [22] E. . E. I. Alliance, *EIA 232, ANSI/EIA/TIA-232-F-1997*, Electronic Industries Alliance, 1997.
- [23] W. Leeb, *Photonik und optische Nachrichtentechnik Vertiefung, Script VO 389.084*, Institute of Communication and Radio-Frequency Engineering, Vienna University of Technology, 2005.
- [24] Browave Corporation., 8-channel CWDM multiplexer specifications. (2006). [Online]. Available: www.browave.com
- [25] FOCI Fiber Optic Communications Inc., 3dB optical splitter Ser.Nr.00007226 datasheet. (1999). [Online]. Available: www.foci.com.tw
- [26] Corning, SMF28-e fiber, datasheet. (2004). [Online]. Available: www.corning.com
- [27] F. Fidler and S. Cerimovic, *High-speed optical characterization of intensity and phase dynamics of a 1.55 μ m VCSEL for short-reach applications*, Optical Fiber Communication Conference, 2006.
- [28] SMPTE, *SMPTE 292M, 1.5 Gb/s Signal/Data Serial Interface*, Society of Motion Picture and Television Engineers, 2008.
- [29] SMPTE, *SMPTE 259M, Television SDTV Digital Signal/Data Serial Digital Interface*, Society of Motion Picture and Television Engineers, 2008.
- [30] SMPTE, *SMPTE 424M, Television 3 Gb/s Signal/Data Serial Interface*, Society of Motion Picture and Television Engineers, 2006.
- [31] SMPTE, *SMPTE 372M, Television Dual Link 292M Interface for 1920 x 1080 Picture Raster*, Society of Motion Picture and Television Engineers, 2002.